

UNCLASSIFIED

AD 295 082

*Reproduced
by the*

ARMED SERVICES TECHNICAL INFORMATION AGENCY
ARLINGTON HALL STATION
ARLINGTON 12, VIRGINIA



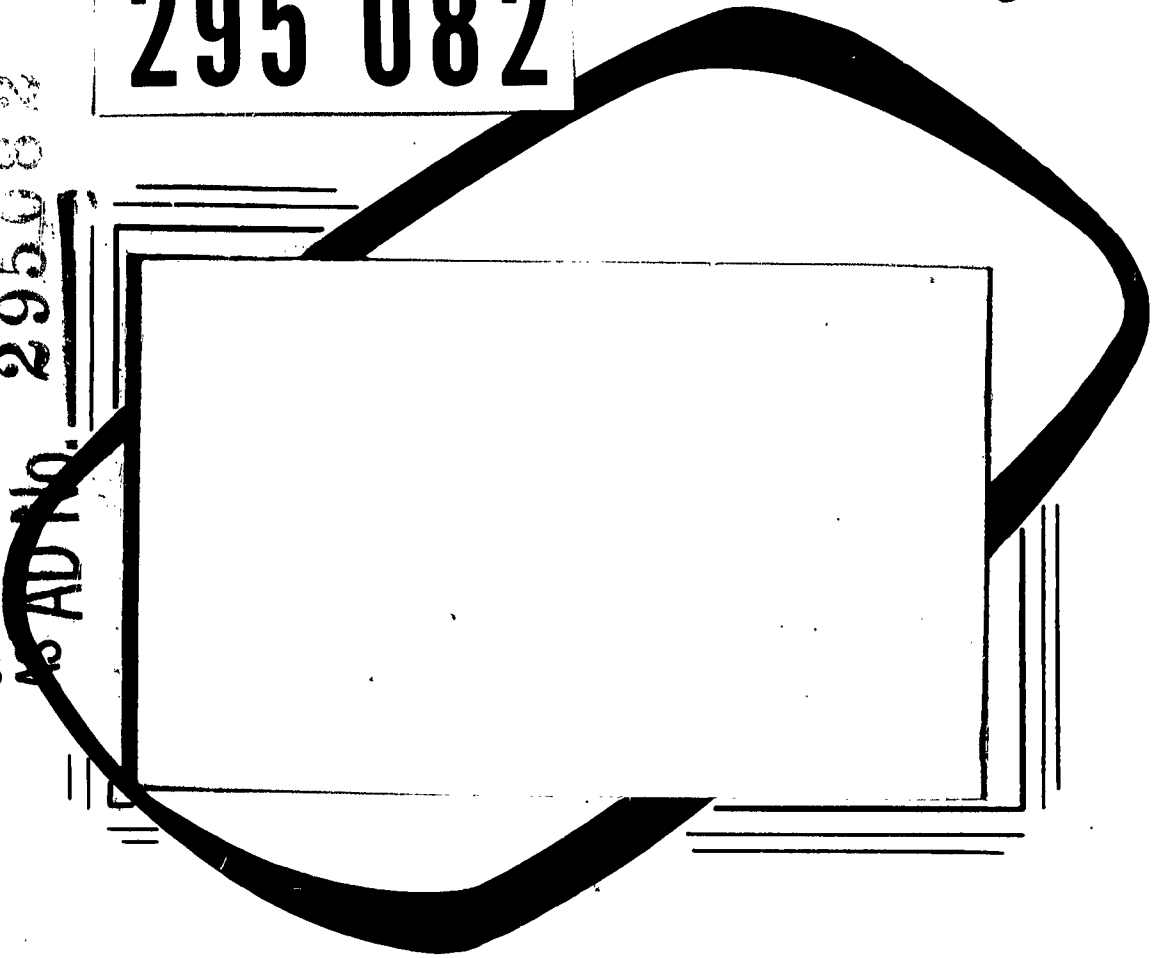
UNCLASSIFIED

NOTICE: When government or other drawings, specifications or other data are used for any purpose other than in connection with a definitely related government procurement operation, the U. S. Government thereby incurs no responsibility, nor any obligation whatsoever; and the fact that the Government may have formulated, furnished, or in any way supplied the said drawings, specifications, or other data is not to be regarded by implication or otherwise as in any manner licensing the holder or any other person or corporation, or conveying any rights or permission to manufacture, use or sell any patented invention that may in any way be related thereto.

63-2-3

295 082

CATALOGED BY ASTIA
No AD No. 295082



ASTIA
RECEIVED
JAN 29 1963
TISIA

THE AEROPHYSICS DEPARTMENT
Of
MISSISSIPPI STATE UNIVERSITY

FLIGHT TESTING OF THE
MARVEL AND MARVELETTE AIRFOIL SECTION

By

Sean C. Roberts

Research Report No. 38

1 May 1962

Conducted For

OFFICE OF NAVAL RESEARCH

Under

CONTRACT NONR 978 (01)

With

SUPPORT PROVIDED BY U. S. ARMY TRANSPORTATION CORPS

By

The Aerophysics Department

Mississippi State University

Reproduction in whole or in part is permitted
for any purpose of the United States Government

TABLE OF CONTENTS

CHAPTER	PAGE
<u>List of Figures</u>	iv
<u>List of Symbols</u>	vi
I. <u>Introduction</u>	1
II. <u>Instrumentation and Construction of the MARVEL</u>	
<u>Glove Section</u>	3
Aircraft	3
Marvel glove section.	3
Angle of attack indicator	5
Pressure measuring equipment	6
Sublimation	7
Sound level equipment	7
III. <u>Flight tests</u>	8
Pressure distributions	8
Angle of attack calibration	8
Surface shear measurements	8
Boundary layer profiles.	8
Sublimation tests	9
Profile drag measurements	9
Sound level measurements	10
Flight testing techniques	10
IV. <u>Presentation of Data</u>	11
V. <u>Discussion</u>	16
VI. <u>Conclusions</u>	23

REFERENCES	25
FIGURES	26

LIST OF FIGURES

<u>Figure</u>		<u>Page</u>
Figure 1.	General view of the TG-3A with the glove section on the port wing	28
Figure 2.	A flight photograph of the glove section from the cockpit	28
Figure 3.	Construction photograph of the glove section showing rib spacing	29
Figure 4.	Construction photograph of the glove section showing removable panel, fiberglass skinning and the blowers	29
Figure 5.	The integrating wake rake used in the profile drag measurements	30
Figure 6.	Wing tip photograph of the angle of attack system	30
Figure 7.	Sublimation photograph showing laminar flow to 50% chord, $U_{\infty} = 70$ mph, $C_L = 0.51$, $\alpha = 4.7^\circ$	31
Figure 8.	Sublimation photograph showing leading edge bubble. $U_{\infty} = 42.5$ mph, $C_L = 1.2$, $\alpha = 16.3^\circ$	31
Figure 9.	Enlarged view of boundary layer mouse and scale	32
Figure 10.	Sensitive pressure gauge, 0 - 0.5 inches water.	32
Figure 11.	Microphone pick-up probe on the glove section.	33
Figure 12.	The sound level meter and the frequency filter box in the cockpit.	33
Figure 13.	Pressure distributions around the MARVEL airfoil section (experimental and theoretical results)	34
Figure 14.	Airfoil section lift coefficient against indicated airspeed	35
Figure 15.	The angle of attack indicator calibration curve.	35
Figure 16.	Airfoil section lift coefficient against angle of attack (experimental and theoretical curves)	36

Figure 17.	Pitching moment coefficient curves	37
Figure 18.	Profile drag curve, MARVEL airfoil section	38
Figure 19.	Surface shear curves at various angles of attack	39
Figure 20.	Profile drag breakdown into skin friction and pressure drag components.	40
Figure 21.	Chordwise development of δ^* , Θ , and H on the upper surface of the glove section	41
Figure 22.	Chordwise distribution of sound level intensity	42
Figure 23.	Transition curves, upper surface of glove section	43
Figure 24.	Sound level intensity boundary layer profiles at various airspeeds and frequencies recorded at the 90% chord position on the upper surface	44
Figure 25.	Height of the boundary layer above the surface at various airspeeds at the 90% chord position.	45
Figure 26.	Possible solution to the leading edge separation problem; drooped leading edge	46

LIST OF SYMBOLS

$x - y$	Coordinates
U	Local velocity in ft/sec
p	Static pressure
H	Total head
ρ	Density of air
C_p	Pressure coefficient = $1 - \left(\frac{U}{U_\infty}\right)^2$
α	Angle of attack in degrees
L	Lifting force
D	Dragging force
S	Periphery of an airfoil
F	Friction force
C_L	Lift coefficient
S	Wing area
C_{D_0}	Profile drag coefficient
τ_0	Shearing force
C	Airfoil chord
μ	Viscosity of air
δ^*	Boundary layer displacement thickness = $\int_0^\infty \left(1 - \frac{u}{U}\right) dy$
Θ	Boundary layer momentum thickness = $\int_0^\infty \frac{u}{U} \left(1 - \frac{u}{U}\right) dy$
H	Boundary layer parameter = $\frac{\delta^*}{\Theta}$
f	A factor for profile drag measurements
w	Height of wake rake
db	Sound level intensity in decibels

U_{τ}	Friction velocity	ft/sec
A. B.	Turbulent boundary layer wall law constants. $A = B = 5.6$	
ν	Kinematic viscosity	
d	Internal diameter, inches	
C_M	Pitching moment coefficient	
C_{MO}	Pitching moment coefficient about any point of chord when $C_L = 0$	

Subscripts

∞	Free stream conditions
i	Indicated conditions
w	Wake conditions
av.	Average conditions
L	Local conditions
Le.	Leading edge
ac.	Aerodynamic center

INTRODUCTION

The MARVEL aircraft was designed as an STOL aircraft with high cruise performance capabilities. The most important regime of flight on such an aircraft is the low speed, high lift coefficient range. The low stalling speed of this aircraft dictated a rectangular planform with little sweep to ensure lateral control with the wing partially stalled. Airfoil sections for low speed flying need to be highly cambered with the point of maximum camber well forward to ensure low pitching moments and smaller tailplane requirements whereas for maximum cruise speeds, a thin low-cambered airfoil is required. To satisfy both requirements, a compromise was reached in the form of a variable cambered airfoil. The uncambered airfoil was an excellent airfoil for the cruise condition due to its low drag and when cambered, the airfoil was very suited to high lift coefficient flying. To ensure maximum utilization of the fully cambered wing, a turbulent high lift boundary layer control system is necessary to prevent turbulent boundary layer separation. The airfoil when designed was a combination of low drag airfoil sections both forward and aft of the spar with an increase in leading edge radius in an attempt to prevent laminar separation at high angles of attack. When the airfoil is in the cambered position, however, only the section forward of the spar retains its original shape and with the flight loads on the relatively flexible wing, it would be difficult to pin down the exact coordinates of the airfoil. Fortunately, small changes in airfoil shape are unimportant in this case unless they are so abrupt as to be considered discontinuities because the high

lift boundary layer control system should be able to cope with small changes in airfoil section. However, the shape of the uncambered airfoil in the high speed or cruising condition is very important if either a laminar BLC system or a low shear BLC system is to be applied.

No previous wind tunnel or flight tests have been performed on this airfoil section and all data used in the aircraft design was obtained from theoretical considerations using such tools as the Fourier analysis technique for determining pressure distributions and lift coefficients from aircraft coordinates and profiles drags from boundary layer theory. One object of this report is to make a comparison between the theoretical and experimental results. Although it would have been possible to perform model tests in a wind tunnel, the results would have been very inconclusive due to a lack of similarity between model and wing in construction. Blockage, wall proximity and Reynolds Number effects on the boundary layer data would also entail considerable corrections to the results. The solution to the problem was to make a model at least full size and test it at flight Reynolds numbers on an aircraft. The airfoil model was made in the form of a cuff or a glove section which fitted over the original wing of a TG-3 sailplane and extended from the fuselage to a boundary layer fence. The contents of this report deals with flight testing of this MARVEL airfoil glove section.

INSTRUMENTATION AND CONSTRUCTION OF THE MARVEL GLOVE SECTION

Aircraft

The aircraft used in these tests was a Schweizer TG-3 sailplane which had a fiberglass airfoil glove section fitted on the port wing. The glove section extended from the fuselage to a boundary layer fence 80 inches from the wing root section (Figure 1). The aircraft had an empty weight of 1100 pounds and normally carried a pilot and observer. The airspeed total head was taken from a Kiel tube mounted on the fuselage nose and the static from a static tube which was mounted on top of the vertical stabilizer. The system was dynamically balanced and static position error determined by comparison with a trailing static bomb. The port wing over which the glove section was constructed was divided into three spanwise compartments, each with its separate blower, venturi meter and respective controls.

The Marvel Glove Section

The chord of the NACA 4416 section which is the airfoil on the sailplane was 60 inches whereas the MARVEL airfoil had a maximum chord of 54.98 inches, therefore, to superimpose a MARVEL glove section on the original airfoil, it was necessary to increase the size of the airfoil section by an appropriate factor. To ensure adequate spacing between the original section and the glove section for internal flow of the boundary layer control systems it was necessary to increase the original MARVEL airfoil section by a factor of 1.4 which increased the chord to 6.4 feet. The original

NACA 4416 airfoil on the TG-3 had a test section extending from 2 feet from the wing root to 6 1/2 feet from the wing root but the MARVEL glove section was constructed from the outer edge of the original test section to the fuselage and with the help of a boundary layer fence at the outer edge, three-dimensional effects were minimized. Although the MARVEL wing would have some taper, it was decided for simplicity of construction to make the glove section with a constant chord.

As the MARVEL and MARVELETTE wings would be constructed of fiberglass, it was decided to build the glove section in a similar manner to these wings in such things as material, rib spacing and skin thickness so that porosity tests could be completed. Fiberglass ribs fabricated using a steel mold were made up and glued to the original ribs of the section. The fiberglass skin was made up and allowed to cure for two months before using and extra ribs were placed between the original ribs to ensure that the maximum rib spacing did not exceed three inches. The three original compartments were sealed into the new section and another leading edge compartment added so that suction could be applied ahead of the 30% chord position of the glove section. A removable panel was incorporated on the bottom side of the glove to allow access to the blowers and the inside of the compartments. The cured .050" thick top skin was put on the test section in two sections, each approximately 40" wide and extending from the beginning of the removable panel on the bottom side, around the leading edge to the trailing edge of the top surface. A chord-wise panel extended from the back of the removable panel to the trailing edge of the section on the bottom surface. The removable panel fitted very snugly into a joggled surrounding skin and was held in place by

wood screws. This method of skinning eliminated all spanwise joints on the top surface the only joint being chordwise. All small gaps were carefully filled and the entire section primed and painted white.

By means of a waviness gauge it was found that the maximum depression or hump on the top surface was less than .001". Thirty-eight flush pressure taps were built into the section on the top and bottom surfaces and their positions marked on the boundary layer fence in percent chord (Figure 2). A calibrated venturi quantity flow meter was installed at the entrance of each blower in its separate compartment and the static taps as well as the wing internal pressure taps were routed to the cockpit and connected to airspeed indicators. The internal compartment statics were connected against the aircraft total head.

Angle of Attack Indicator

Various types of angle of attack indicators were tried including vanes which rotated variable resistors and capacitors which were connected to balanced bridges and measured. Unfortunately, the friction between the movable arm and the resistance coil was sufficient to cause considerable hysteresis in the results. The variable capacitance type eliminated the friction problem but the change in capacitance for the small angles involved was very small making accurate measurement difficult. A number of other systems including an optical method were considered but the simplest and most direct approach to the problem was found to be the only one to give consistent results. This angle of attack indicator consisted of a large vane painted black, three feet long mounted three feet above a six-foot boom on the front of the aircraft. A large

black line was painted on the side of the fuselage parallel to the zero angle of attack line of the glove section (Figure 6). A camera mounted on the wing tip when activated from the cockpit took a picture of the vane and the painted line on the fuselage. To find the angle of attack, the negative was projected onto a white screen and lines drawn through both the vane and the line on the fuselage and the angle between them measured. This measured angle was the angle of attack of the glove section to the freestream for that particular flight condition.

Pressure Measuring Equipment

Kollsman helicopter airspeed indicators were used when a few pressure readings were needed but when pressure distributions or boundary layer profiles were recorded, a twenty channel photographic manometer was used. Surface shear was measured using the Preston Method which consisted of a total head tube resting on the surface and a static tube which sensed the local pressure. The reading in miles per hour on an airspeed indicator connected across the pitot-static system is a function of surface shear for an impervious surface. Boundary layer velocity profiles were measured using small total head tubes and a local static pressure tap connected to a water manometer, the y values were determined by placing a scale beside the total head tube and photographing from the front (Figure 9). Profile drag of the test section was measured by means of an integrating wake rake (Figure 5) which was connected to a trailing static bomb and the difference between the aircraft airspeed and the average wake rake total head across a sensitive pressure measuring instrument (Figure 10) the aircraft airspeed being obtained from the aircraft total head

and a trailing static.

Sublimation

Sublimation tests were carried out by spraying a naphthalene ether solution onto a black painted surface immediately prior to take-off and photographing from the cockpit in flight. To prevent the test section being permanently black, a separating film of polyvinyl alcohol was sprayed onto the section before the black paint was applied.

Sound Level Equipment

The microphone pick-up probe was incorporated in a small streamlined bomb (Figure 11) which was attached to the upper surface of the airfoil section. The microphone output was fed into a frequency filter unit which had frequency filters at 800, 1000, 1200, 1400, 1600, and 2000 c/s with a range of 4.0% and then to a General Radio sound level meter which indicated the RMS value of the fluctuations. A loudspeaker was incorporated in the system with the output from the frequency filter which enabled a monitoring of the sound level equipment and when the microphone probe was mounted at the 80% chord position, it was an excellent stall warning indicator when the boundary layer was separating from the surface.

FLIGHT TESTS

Pressure Distributions

The static taps on the glove section were connected to a photographic multi-channel water manometer against the aircraft total head. Pressure distributions were recorded at altitudes ranging from 15,000 feet to sealevel and airspeeds from 42.0 mph to 100 mph enabling possible Reynolds number effects to be determined.

Angle of Attack Calibration

As the angle of attack indicator was not a direct reading type, it was necessary to calibrate the airspeed system for angle of attack with a constant aircraft weight. Ensuring a constant all-up weight on a sailplane is very simple as there is no fuel on board. Wing tip photographs of the vane and the chordline painted on the side of the fuselage were taken at various airspeeds and altitudes, the negatives projected onto a screen and the angle of attack of the glove section determined.

Surface Shear Measurements

Preston shear meters were taped to the surface of the airfoil and connected to airspeed indicators in the cockpit. The airspeed readings in miles per hour which are functions of local surface shear were recorded at various airspeeds and altitudes.

Boundary Layer Profiles

The total head tubes of the boundary layer mouse were connected

against the local static pressure across a photographic water manometer. The mouse was taped to the surface and boundary layer profiles taken at various airspeeds. The above procedure was repeated for all chordwise positions on the glove section.

Sublimation Tests

The MARVEL glove section was prepared for the sublimation tests as in the previous chapter and immediately prior to take-off, naphthalene in petroleum ether solution was sprayed on the surface. The test section was photographed whenever flow patterns formed at the particular flight conditions. Whenever the test speed was very much different from the towing speed, the section was covered after spraying with sheets of brown paper which protected the naphthalene from the air flow. When the flight conditions were set up after release, the paper was torn off by means of a wire and the necessary photographs taken. An automatic camera was mounted beside the landing wheel to enable photographs of the bottom surface of the test section to be taken.

Profile Drag Measurements

The two-dimensional profile drag of an airfoil can be measured in flight by means of an integrating total head rake placed in such a manner as to completely span the wake from the airfoil. The principle used is the rate of change of momentum across the airfoil and if we measure the aircraft total head and the average wake total head, it is a simple matter to calculate profile drags. The two airspeed indicators for reading the aircraft and average wake total heads were read simultaneously by photo-

graphic recording for all flight conditions. A few tests were performed with one airspeed indicator reading the aircraft airspeed and a sensitive pressure instrument recording the difference in the aircraft and the average wake total heads.

Sound Level Measurements

The microphone housing and probe (Figure 11) was taped to the wing with the probe resting on the surface and the sound level reading in decibels of the RMS value of the pressure fluctuations at each particular frequency recorded for each flight condition. The above process was repeated with the probe at all chordwise positions on the test section. At the 90% chord position the microphone was taped to the test section with the probe 0.1 inches above the surface and sound level readings taken at every frequency for each airspeed. This was repeated with the probe at various heights above the surface until the probe was obviously in the freestream.

Flight Testing Techniques

Before each flight the altimeter was always set at 29.92 to insure that irrespective of the local barometric pressure, altitude readings from day to day were consistent. Although the aircraft pressure systems were dynamically balanced it was quite impractical to balance such things as pressure taps or boundary layer probes when connected to a manometer, therefore, considerable time had to be spent at each test condition before equilibrium conditions were established and the pressure readings recorded. Due to the lack of symmetry of the aircraft, it was necessary to apply

corrective ailerons and rudder to maintain a zero sideslip condition for each flight condition.

PRESENTATION OF DATA

When local static pressure is balanced against aircraft total head Bernoulli's equation gives

$$p + 1/2 \rho U^2 = p_{\infty} + 1/2 \rho U_{\infty}^2$$

for which

$$U = \sqrt{\frac{p_{\infty} - p}{\frac{1}{2} \rho}} = \sqrt{\frac{2 \Delta p}{\rho}} \quad (1)$$

which can be reduced to $U_{ft/sec} = 66.1 \sqrt{\Delta p}$ where Δp is measured in inches of water.

Δp is read directly from the water manometer and using the above equations velocity distributions are obtained and from these curves it is a simple step to obtain pressure distributions using the equation

$$C_p = 1 - \left(\frac{U}{U_{\infty}}\right)^2 \quad (2)$$

Experimental pressure distributions are plotted against x/c and compared with the theoretical distributions obtained from the Fourier Analysis technique (Figure 13).

Angles of attack in degrees were plotted against indicated airspeed and a reasonable curve drawn through these points which were obtained using the wing tip camera. Experimental points obtained by photographing the sailplane from the Stearman Tug aircraft are also shown in Figure 15.

By using the pressure distributions and the angle of attack results, section lift and pressure drag curves were obtained by the following methods. If p is the normal force on the airfoil and θ the angle between the tangent

to the surface and the undisturbed wing direction, then

$$\delta L = (P \cos \theta + F \sin \theta) \delta S$$

and

$$\delta D = (-P \sin \theta + F \cos \theta) \delta S \quad (3)$$

where F is the local friction force acting on the airfoil.

The vertical component of the friction force is very small in comparison to the pressure forces, therefore,

$$C_L = \frac{\oint (P \cos \theta) ds}{\frac{1}{2} \rho U_\infty^2 S} \quad (4)$$

Curves of C_L against V_i and C_L against α are plotted in Figure 14.

$D = \oint (-P \sin \theta + F \cos \theta) ds$ can be computed by a numerical step by step method or it can be obtained graphically by projecting a horizontal scale from a vertical line drawn through the projected lines. The enclosed area is a function of the pressure drag coefficient $C_{D0(\text{pressure})}$. Curves of $C_{D0(\text{pressure})}$ against α are plotted in Figure 20.

Pitching moment coefficient curves were obtained from the pressure distributions by the following method.

$$C_{M_{LE}} = C_{M_0} - C_L X_{ac} \cos \alpha - C_D X_{ac} \sin \alpha \quad (5)$$

For moderate angles of incidence:

$\cos \alpha = 1$, $C_D \sin \alpha$ is small and can be neglected.

$$\therefore C_{M_{LE}} = C_{M_0} - C_L X_{ac} \quad (6)$$

$$\frac{dC_{M_{LE}}}{dC_L} = \frac{dC_{M_0}}{dC_L} - X_{ac}$$

but as $\frac{dC_{M_0}}{dC_L} = 0$ by definition

$$\text{Then } X_{ac} = - \frac{dC_{M_{LE}}}{dC_L} \quad (7)$$

According to Preston the corrected calibration for round total head tube on the surface to determine surface skin friction is

$$\text{Log} \frac{\tau_o d^2}{4 \rho v^2} = -1.366 + 0.877 \text{Log}_{10} \frac{(\frac{1}{2} \rho U_L^2) d^2}{4 \rho v^2} \quad (8)$$

U_L is read directly from the Preston tube airspeed indicator and knowing the internal diameter of the tube and the altitude of the aircraft, it was possible to calculate τ_o at all chordwise stations and flight conditions. Curves of τ_o against x/c are plotted in Figure 19. From these curves, a crossplot of transition points against indicated airspeed was obtained (Figure 23). The transition point was taken to be that point where the surface shear suddenly increased.

The velocities in the boundary layer were calculated from the water manometer readings using equation (1) and the "y" values determined from the enlarged photograph of the boundary layer mouse and scale (Figure 9). Boundary layer velocities profiles were drawn from which δ^* , θ , and H were calculated and plotted against x/c (Figure 21). And from these curves, transition points were obtained and plotted in Figure 23. The transition was taken to be where $H = 2.6$ which was considered to be the critical value for transition. Surface shear was determined from the boundary layer profiles using the Wall Law Technique from turbulent boundary layer theory.

$$\frac{u}{U_T} = A + B \text{Log} \frac{y U_T}{v} \quad (9)$$

$$\text{where } A = B = 5.6$$

U_T can be found by plotting u/U_T against $\log \frac{y U_T}{v}$ and adjusting U_T until the Wall law region falls on the line $5.6 \log \frac{y U_T}{v}$. As this involves an iterative method which could be quite tedious an alternative direct method was used.

Add $B \log u/U_\tau$ to both sides of the Wall Law equation

$$\begin{aligned} \frac{u}{U_\tau} + B \log \frac{u}{U_\tau} &= A + B \log \frac{yU_\tau}{\nu} + B \log \frac{u}{U_\tau} \\ &= A + B \log \frac{yu}{\nu} \end{aligned} \quad (10)$$

$$\therefore \frac{u}{U_\tau} = f\left(A, B, \frac{yu}{\nu}\right) \quad (11)$$

From equation (10) a curve of u/U_τ against $\frac{yu}{\nu}$ was plotted and tabulated and for each boundary layer point $u(y)$ a value of u/U_τ and hence U was found. U_τ was plotted against y and in the Wall Law region U_τ should be a constant and that constant value of U_τ was the friction velocity for the profile. The values of τ_0 obtained from the boundary layer profiles were added to the skin friction curves (Figure 19) obtained using the Preston tube method.

The two-dimensional drag was measured using an integrating total head wake rake balanced against a trailing static, giving a reading of an airspeed indicator U_w .

$$C_{D_0} = f \frac{\omega}{c} \int \frac{H_{\infty} - H_w}{H_{\infty} - p_{\infty}} dy = f \frac{\omega}{c} \left(\frac{H_{\infty} - H_{w_{ar}}}{H_{\infty} - p_{\infty}} \right) = f \frac{\omega}{c} \left(\frac{\frac{1}{2} \rho U_0^2 + p_{\infty} - \left(\frac{1}{2} \rho U_{w_{ar}}^2 + p_w \right)}{\frac{1}{2} \rho U_0^2} \right) \quad (12)$$

and in this case where $p_0 = p_w$ due to the trailing static

$$C_{D_0} = f \frac{\omega}{c} \left(\frac{U_0^2 - U_{w_{ar}}^2}{U_0^2} \right) \quad (13)$$

The value of "f" in the above equation is a function of airfoil thickness, distance of rake behind trailing edge and distance from the fuselage

side and can be calculated for each case using reference 1 by Silverstein and Katzoff. Curves of C_{D_0} against α were plotted (Figure 18).

The sound level measurements were plotted in the form decibels against percent chord at each frequency for every airspeed and from the curves where the sound level rose abruptly a transition point was taken and plotted in Figure 23. At the 90 percent chord position sound level boundary profiles were taken and plotted as db against y for each frequency and aircraft airspeed (Figure 24), and a crossplot of y against U_0 drawn where y was obtained from the point where its sound level sharply decreased indicating freestream conditions.

From the sublimation photographs transition points at every airspeed were determined and plotted on Figure 23 for comparison with other methods of transition detection.

DISCUSSION

The fiberglass construction of the glove section stood up very well to the rigors of six months of continuous testing and flying. The beautifully smooth finish, absolutely wave-free would have been extremely difficult to attain by any other means of construction except perhaps by machined metal skin supported on an adequate honeycomb material which, of course, would have been extremely costly in comparison to the fiberglass construction. The low weight of the fiberglass glove section was an important factor considering that the glove was on one wing only. The fiberglass glove section was easily repaired and the addition of such things as drooped snoots to the leading edge was a simpler operation than it would have been with a metal skin. The biggest disadvantage with fiberglass is that it tends to move with high temperatures, and it is necessary in countries where it is relatively warm that the finished construction is painted white to reduce the heat absorption of the fiberglass. In some of the tests where a black surface was required, for example in the sublimation tests, it was necessary to ensure that the tests were completed early in the morning before the sun rose high in the sky, otherwise the section would warp quite considerably. The skin between the ribs after a period of months did tend to sag a little, but this could be eliminated by extensive curing of the skin before applying to the finished structure.

As discussed in the instrumentation section of this report a number of angle of attack indicators were tested with varying degrees of success, and the most consistent method was found to be an indirect method using a free

vane and a wing tip mounted camera. Attempts were made to photograph the system from the accompanying tug aircraft but as can be seen from Figure 15, this method incorporated a number of errors such as parallax due to photographs being taken from different angles, and also the effect of the proximity of the accompanying aircraft was quite considerable. Using the wing tip system results were repeatable to within $1/4^\circ$, which is reasonable. A more sophisticated system using variable resistances on a smaller vane could be made using some special potentiometer which requires very little torque to vary the resistance so that the hysteresis effects are minimized. The accuracy of the $U_i - \alpha$ curve was shown by the fact that the $C_L - \alpha$ curve is a straight line (Figure 16).

The experimental pressure distributions shown in Figure 13 are very smooth, and they clearly indicate that the MARVEL airfoil section was obviously designed as a laminar flow section because of the absence of sharp peaks in the distributions at small angles of attack and the pressure peak, or more precisely, the region of minimum pressure extends as far aft as 40% chord. This means that boundary layer transition to turbulent flow would be delayed until the region of adverse pressure gradient is reached if the surface is smooth enough to prevent premature transition. This is verified by the transition curves in Figure 23. The theoretical pressure distributions obtained from the airfoil coordinates using a Fourier analysis technique agree very well with the experimental results for the upper surface for angles of attack up to about 5° . There is a discrepancy at the leading edge with the theoretical results indicating a pressure peak about the 5% chord position which does not exist experimentally also considerable disagreement occurs at the trailing edge. This breakdown of the theory at the

leading and trailing edges is typical of the Fourier analysis technique for calculating pressure distribution, and unfortunately the leading edge results are very important for most types of boundary layer control theories. The differences between theoretical and experimental results on the bottom surface are less significant than the leading edge differences because they have less effect on boundary layer control theories, nevertheless the differences are so great that considerable care should be taken when using this method of either designing an airfoil for a given pressure distribution or vice versa. At angles of attack greater than 5° the difference in theoretical and experimental results, especially at the leading edge, increases. It is probably the leading edge discrepancy at high angles of attack which causes the difference further aft on the upper surface of the airfoil section. The errors incorporated in the Fourier method of pressure distribution calculation seem to increase quite considerable with increase in angle of attack and it appears that the use of this method in calculating a high lift boundary layer control system where the airfoil is at large angles of attack is open to question. This discrepancy may be the reason that Mississippi State University had some difficulty in accurately calculating high lift boundary layer control systems. The section lift coefficient against angle of attack curves plotted in Figure 16 show the considerable difference between the experimental and theoretical results. The experimental curve shows a loss of linearity at approximately $\alpha = 16^\circ$ which corresponds to the formation of a leading edge laminar separation bubble at the 2% chord position and a boundary layer separation at 90% chord position. The theoretical results being obtained from a potential flow theory do not show any boundary layer viscous flow problems such as separation at the leading

and trailing edges and a tendency for the airfoil to stall at large angles of incidence. The difference in $dC_L/d\alpha$ obtained from both methods is of the order of 50% which is not really acceptable for further application in boundary layer control theories. It is interesting to note, however, that although the two curves are very different, they both converge on the $C_L = \text{zero}$ line indicating that the zero lift incidence is -3.75° . The pitching moment coefficient curves (Figure 10) which were obtained by integrating the moment about the leading edge of the pressure distributions show better agreement especially in the position of the aerodynamic center which is a function of the slope of the curve. The values of C_{M_0} , which is the pitching moment coefficient when the lifting force is zero, show the same order of error as the $dC_L/d\alpha$ results, notably 50%. The bending up of the experimental curve to a positive slope at high values of C_L indicate that the airfoil is unstable as the stall is approached. This instability is quite normal and together with the usual fuselage instability is corrected by the action of the tailplane.

The profile drag curves obtained using an integrating wake rake method are shown on Figure 18, and it can be seen that the section drag coefficient is quite low dropping to the order of .005 at cruising incidences of 2° and Reynolds numbers of the order of six million. The low drag is mainly due to the large regions of laminar flow which extend as far aft as 50% on the top surface. The breakdown of the profile drag (Figure 20) shows that the skin friction drag contributes about 55% of the total profile drag the remaining drag being due to pressure forces. The skin friction drag was determined experimentally using Preston tubes and also from boundary layer profiles from which U_τ and hence, τ_w were calculated

using the Law of the Wall technique. The curves of τ_o against x/c are plotted in Figure 19, and a comparison of the methods made. The skin friction drag was found by integrating the τ_o curves obtained from the Wall Law method.

A number of methods were used in determining transition although some of the methods gave transition results as a by-product of their main purpose, which in the case of the surface shear results is the determination of skin friction drag. The only method used primarily for transition detection was the sublimation technique. The transition points taken from the surface shear curves, the sound level curves, and the chordwise variation of H parameter curves are clearly marked on the respective curves; and all these points were transposed to Figure 23, which shows a comparison of the various techniques of transition detection. The agreement in all cases is very good except perhaps in the very low speed region where the leading edge laminar separation bubble was formed. Laminar flow on the upper surface existed back to 45% chord up to angles of attack of six degrees. Probably the simplest means of transition detection is by the use of Preston tubes which give functions of the local surface shear; they are simple to make and arrange on the section, and a direct plotting of the indicated velocity on the airspeed indicators against chordwise position gives transition where the surface shear suddenly increases. A number of these meters can be operated simultaneously by staggering the tubes in a spanwise as well as a chordwise manner. The use of the microphone pickup is also an excellent method if some means of moving the probe chordwise on the surface is available without increasing the upstream surface roughness, the sharp increase in sound level moving from laminar to turbulent flow is very noticeable. The sublimation method can be

tedious as it is necessary to have a black surface so that the naphthalene is clearly visible, and these experiments must be carried out early in the morning before the temperature has risen above about 70° , otherwise the solution tends to sublime as soon as it is applied to the airfoil surface. Nevertheless in regions where flow separations occur, it is an excellent visualization method and as a flow visualization technique it has distinct advantages in that it can be applied to aircraft work where other techniques fail.

Figure 24 shows sound level intensity boundary layer profiles at various airspeeds and frequencies measured at the 90% chord position; the purpose of the profiles was to determine the best pressure fluctuation frequency in a boundary layer at flight Reynolds numbers so that a refined stall warning indicator could be made for the Marvel and Marvelette aircraft. It was necessary to determine the characteristic frequency in a turbulent boundary layer near separation so that a by-pass filter could be installed in the stall warning indicator eliminating all other noises such as those originating in the engine or from aerodynamic sources. By this means the characteristic frequency only is put into the system, and the warning would only be a function of boundary layer separation irrespective of engine or aerodynamic conditions. It seems reasonably clear from Figure 24 that in the 42.5 mph conditions, where the boundary layer is separated at the 90% chord position, that the 1,000 c/s plot gives the sharpest and narrowest indication of the separated boundary layer. This 1,000 c/s result agrees very well with previous wind tunnel results⁵ which indicated either 1,000 c/s or 1,200 c/s as the best frequencies; it, therefore, appears that a by-pass filter at 1,000 c/s with a band width of about 5% would make

an excellent addition to the standard Aerophysics Department stall warning indicator. A crossplot of height of the boundary sound level intensity becomes constant against aircraft airspeed is shown in Figure 25. It is to be noted that the results obtained from different frequencies tend to collapse onto a single curve. Although this is to be expected, it is a reasonable confirmation of the accuracy of the results. From this curve it can be seen that the boundary layer separated quite quickly with a small decrease in airspeed from 55 mph where the boundary layer is 0.7 inches thick to 50 mph where the boundary layer is 1.0 inches thick. Also, it appears that as the airspeed increases and the angle of attack decreases the height of the boundary layer above the surface at the 90% chord position tends to remain constant and the same thing can be said at the low airspeed range where the boundary layer is separated. These boundary layer height results indicate the height the microphone pick up probe must be above the surface at the 90% chord position to indicate boundary layer separation and probable stalling. The above results of course, only hold true when the airfoil has a rear separation stall, and they would be quite meaningless if the airfoil had a leading edge separation stall. Unfortunately, the sublimation photograph shown in Figure 8 indicates a leading edge separation bubble forming at the 2% chord position at an angle of attack of 16 degrees. It is possible that at higher angles of attack this bubble could burst causing a leading edge stall which is very nasty and not to be recommended for slow speed aircraft. To prevent this leading edge bubble forming a number of techniques have been tried but a possible solution to the problem is shown in Figure 26 which is an increase in the leading edge radius resulting in a drooped snoot airfoil. This increase in leading edge radius

decreases the pressure peak and the adverse pressure gradient thereby helping the boundary layer around the leading edge to adhere to the surface.

CONCLUSIONS

The use of fiberglas materials in the construction of the glove section gave a lightweight glove section with excellent surface finish and ease of construction and repair. The surface finish deteriorated with time; small spanwise waves forming between the ribs, it is believed, however, that these can be eliminated by adequate curing of the fiberglas parts before assembly. The main disadvantage with fiberglas is that in hot climates where the temperature can be above 90° F. it is necessary to paint the outside of the assembly white otherwise heat absorption will warp the structure.

The free vane angle of attack system used on the glove section gave consistent results but unfortunately, this type of systems would only be applicable to sailplanes where a constant aircraft weight is easily attained.

The use of the Fourier analysis technique for determining pressure distributions from airfoil coordinates gives reasonable results for the upper surface up to angles of attack of 5°. For angles of attack above 5° the leading edge and trailing edge errors increase until at $\alpha = 15^\circ$ the resulting pressure distribution can have errors up to 50% of the experimental values. Great care should be taken in using this method for calculating low drag boundary layer control systems and in the case of high lift systems where large angles of attack are involved the method is unreliable.

The Marvel airfoil in the imperious uncambered condition is an excellent low drag section with laminar flow extending as far aft as 50% chord at cruising incidences giving section drag coefficients of the order of .005

at Flight Reynolds numbers of 6×10^6 . The section lift coefficient loses its linear relationship with α at $\alpha = 16^\circ$ and this corresponds with the formation of a leading edge laminar separation bubble, but the formation of this bubble could be eliminated by increasing the leading edge radius in which case the airfoil would have a conventional trailing edge stall.

The sound level boundary layer profiles indicate that the best characteristic frequency for a separating turbulent boundary layer is 1,000 c/s and that a by-pass filter at this frequency with a bandwidth of about 5% be used in the construction of a stall warning indicator.

REFERENCES

1. Silverstein, A. and Katoff, S. "A Simplified Method for Determining Wing Profile Drag in Flight", Journal of Aeronautical Sciences, pp. 295-301.
2. Piercy, N. A. V. Aerodynamics. The English Universities Press, Ltd., Chapter 44, pp. 54-58.
3. Cornish, Joseph J., III. A Universal Description of Turbulent Boundary Layer Profiles with or without Transpiration. (Mississippi State University, Aerophysics Department, Research Report No. 29) 1 June 1960.
4. Raspet, A. Improvement of Airfoils by Leading Edge Smoothing. (Mississippi State University, Aerophysics Department) March, 1954.
5. Roberts, Seán C. An Investigation of Two Types of Hole Distribution for Laminar Boundary Layer Control Systems. (Mississippi State University, Aerophysics Department, Research Report No. 37).
6. Smith, D. W. and Walker, J. H. Skin Friction Measurements in Incompressible Flow, NASA TR Report No. 26, 1959.
7. Preston, J. H. The Determination of Turbulent Skin Friction by Means of Pitot Tubes. British ARC Fluid Motion Subcommittee Report No. 15, 758, 31 March 1953.
8. Roberts, Sean C. Suppression of Laminar Separation Bubbles on the Leading Edge of Aerofoils. (Mississippi State University, Aerophysics Department, Research Report No. 39) 1962.

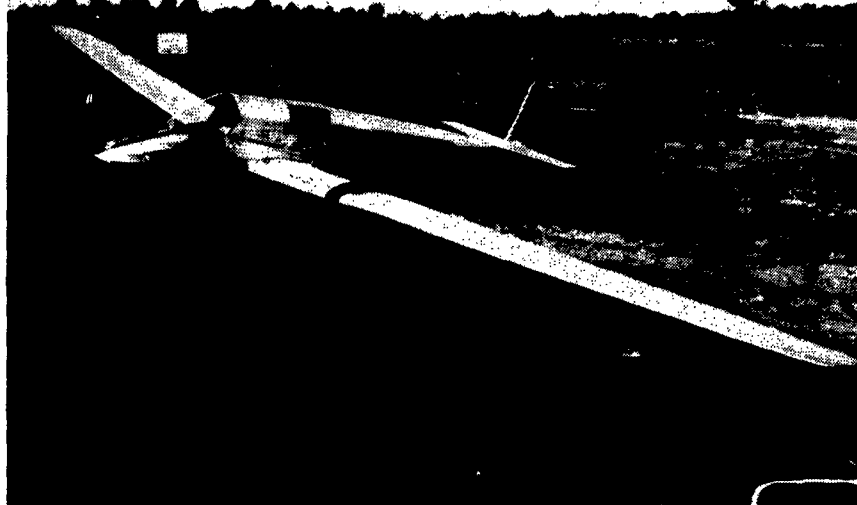


FIGURE 1 GENERAL VIEW OF THE TG-3A WITH THE GLOVE SECTION,
ON THE PORT WING.

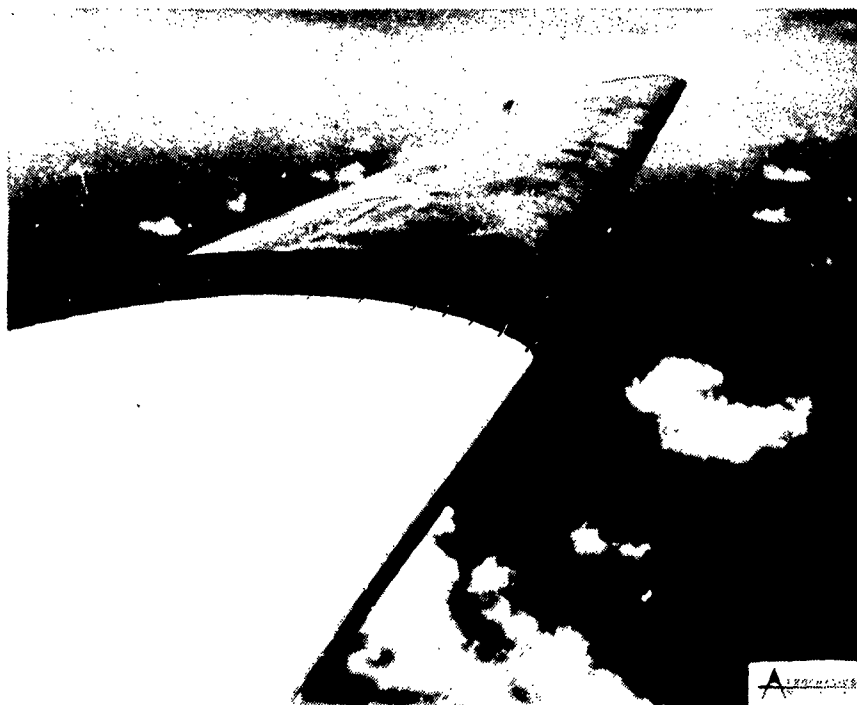


FIGURE 2 A FLIGHT PHOTOGRAPH OF THE GLOVE SECTION FROM
THE COCKPIT.

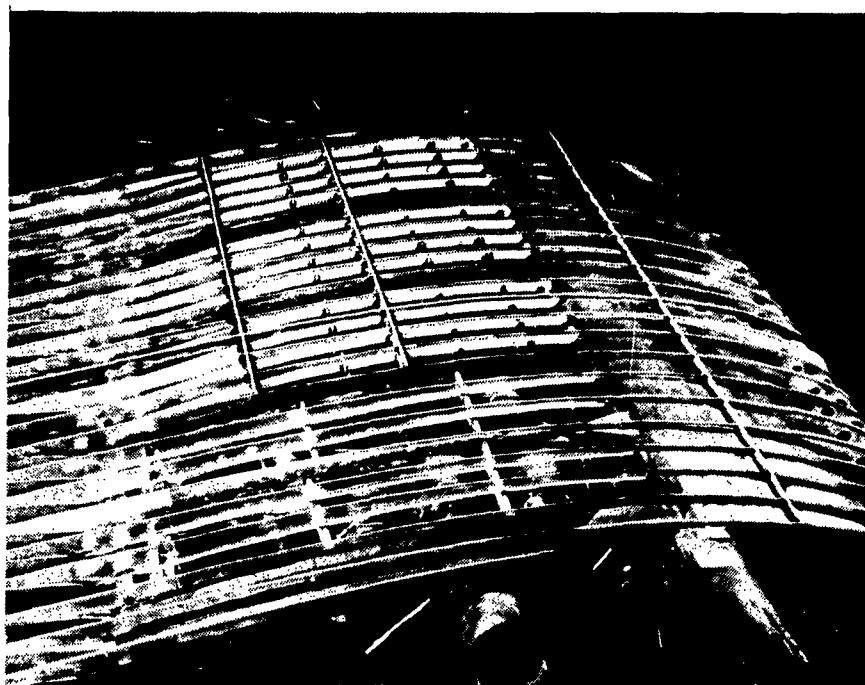


FIGURE 3 CONSTRUCTION PHOTOGRAPH OF THE GLOVE SECTION SHOWING RIB SPACING.

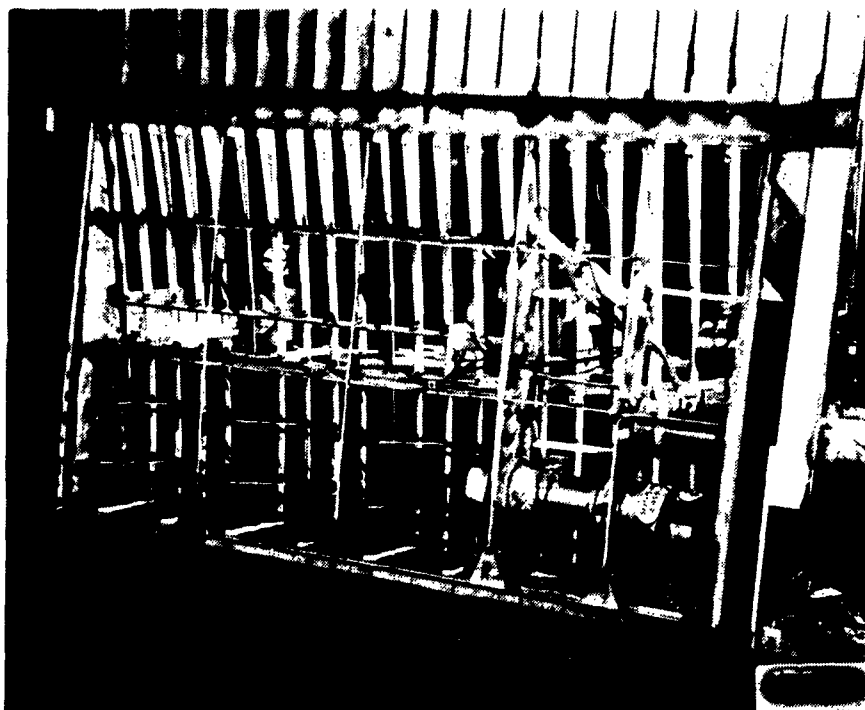


FIGURE 4 CONSTRUCTION PHOTOGRAPH OF THE GLOVE SECTION SHOWING REMOVABLE PANEL, FIBERGLAS SKINNING AND THE BLOWERS.

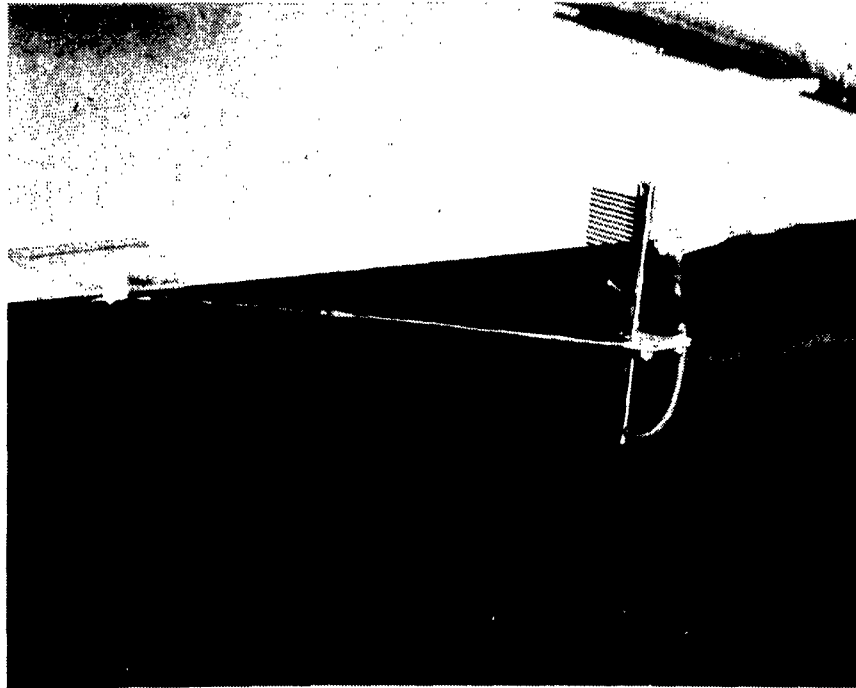


FIGURE 5 THE INTEGRATING WAKE RAKE USED IN THE PROFILE DRAG MEASUREMENTS.

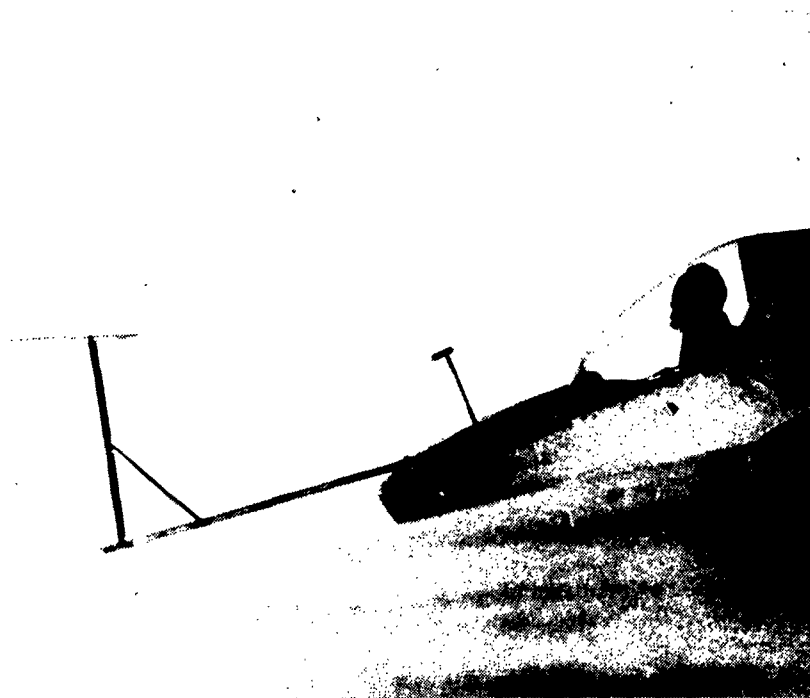


FIGURE 6 WINGTIP PHOTOGRAPH OF THE ANGLE OF ATTACK SYSTEM.

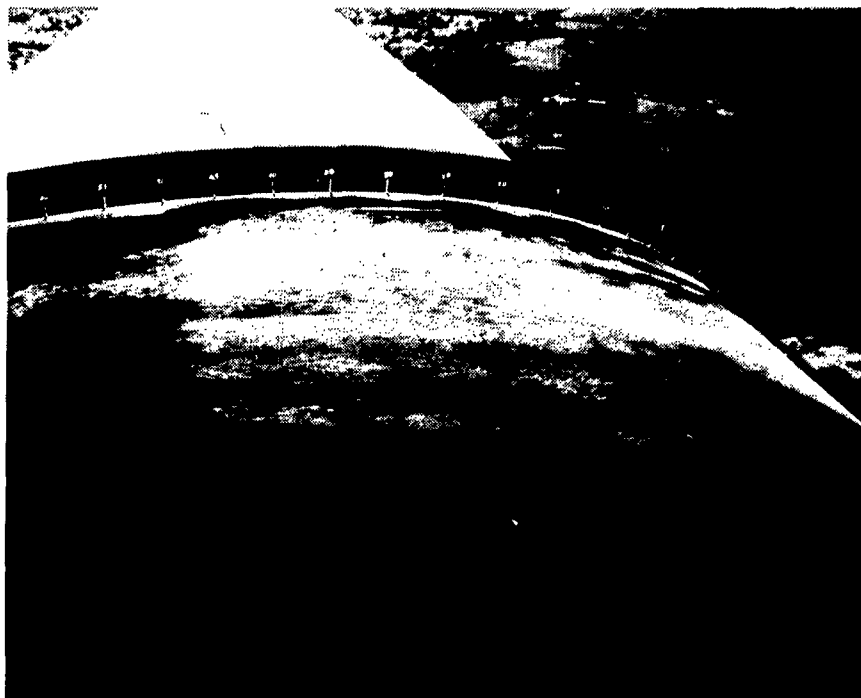
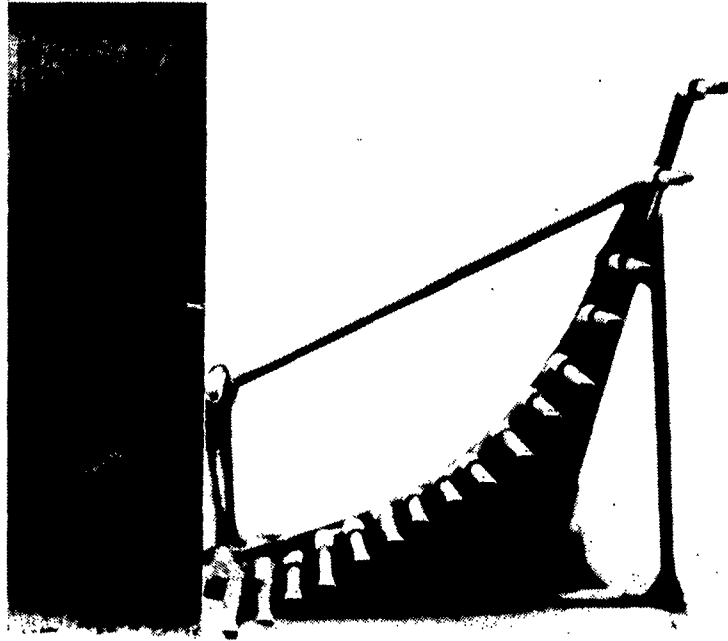


FIGURE 7 SUBLIMATION PHOTOGRAPH SHOWING LAMINAR FLOW TO 50% CHORD, $U_{\infty} = 70$ MPH, $C_L = 0.51$, $\alpha = 4.7^\circ$



FIGURE 8 SUBLIMATION PHOTOGRAPH SHOWING LEADING EDGE BUBBLE, $U_{\infty} = 42.5$ MPH, $C_L = 1.2$, $\alpha = 16.3^\circ$



ALPHAVISION
INTERNATIONAL CORP.
PROVIDENCE, RI

FIGURE 9 ENLARGED VIEW OF BOUNDARY LAYER MOUSE AND SCALE

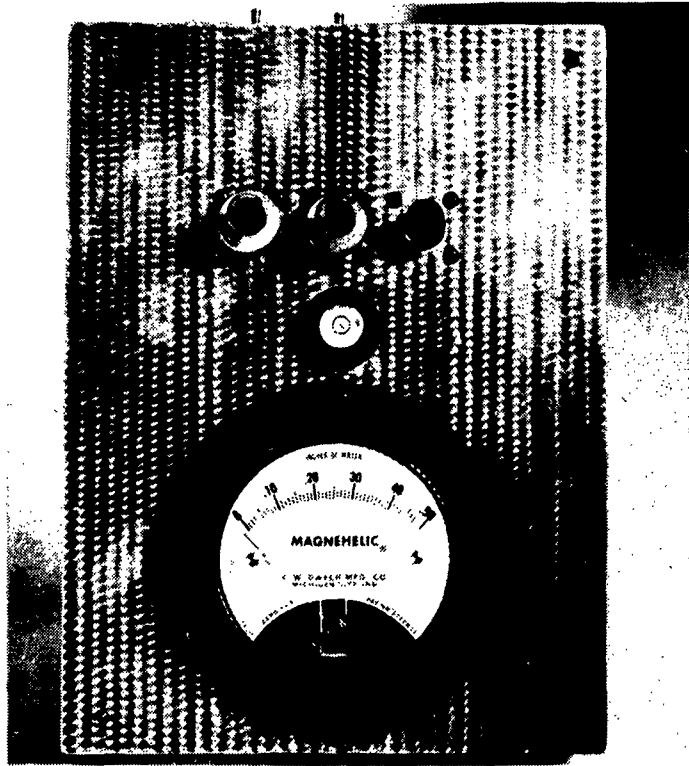


FIGURE 10 SENSITIVE PRESSURE GAUGE, 0 - 0.5 INCHES WATER.

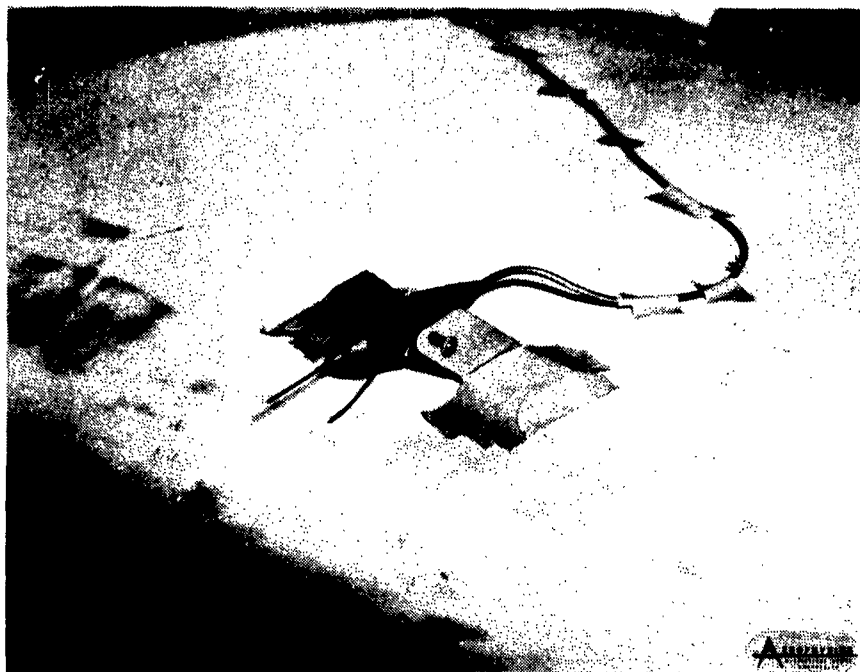


FIGURE 11 MICROPHONE PICK-UP PROBE ON THE GLOVE SECTION.

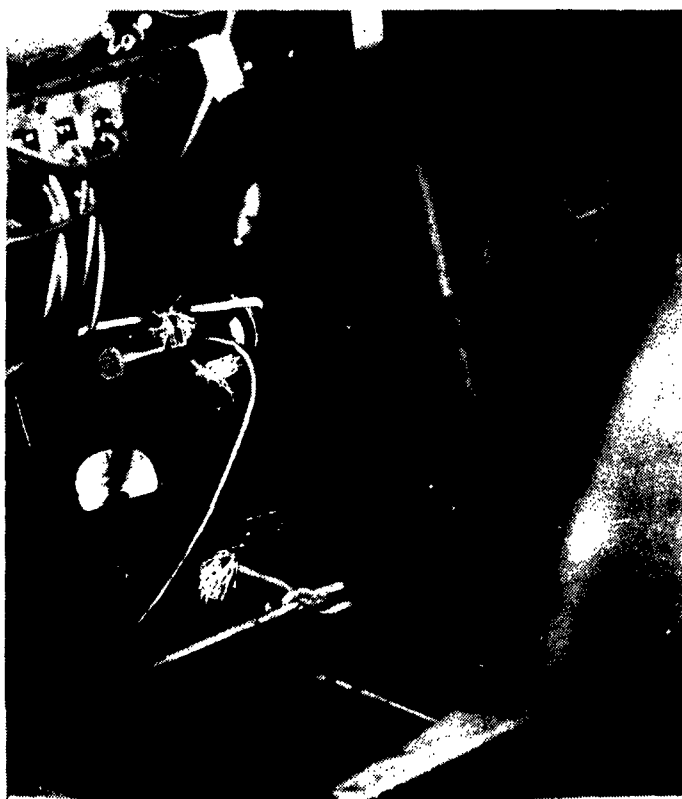


FIGURE 12 THE SOUND LEVEL MEIER AND THE FREQUENCY FILTER BOX IN THE COCKPIT.

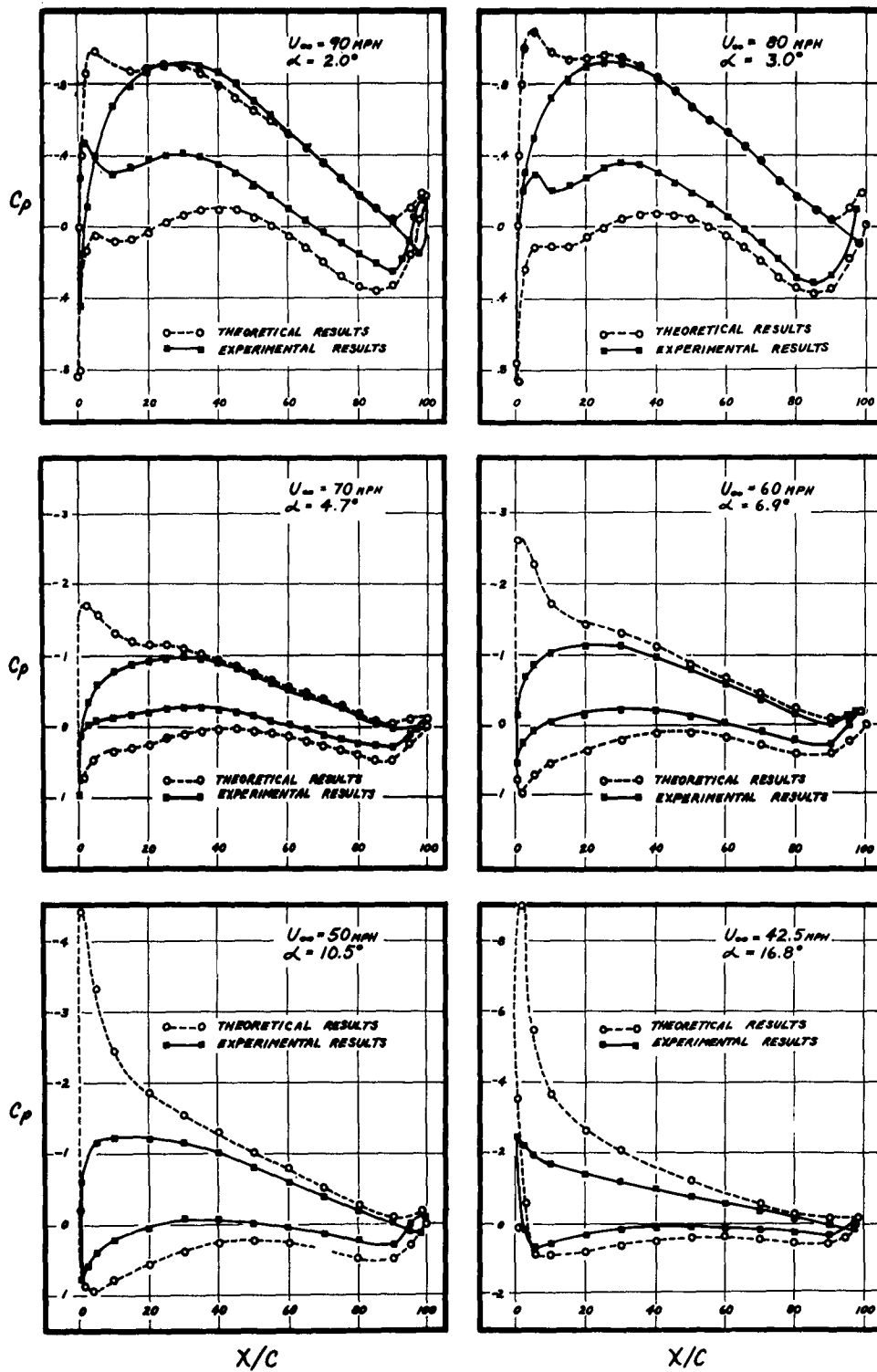


FIGURE 13 PRESSURE DISTRIBUTION AROUND THE MARVEL AIRFOIL SECTION (EXPERIMENTAL AND THEORETICAL-RESULTS)

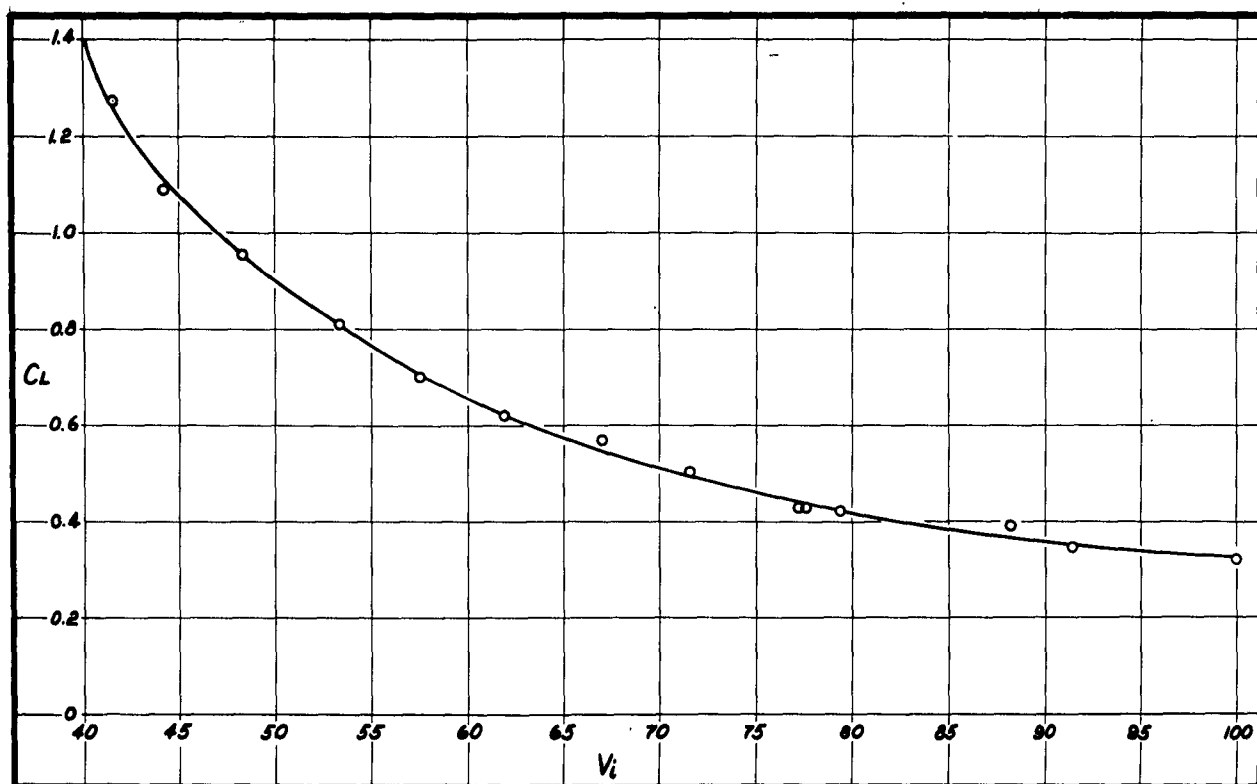


FIGURE 14 AIRFOIL SECTION LIFT COEFFICIENT AGAINST INDICATED AIRSPEED.

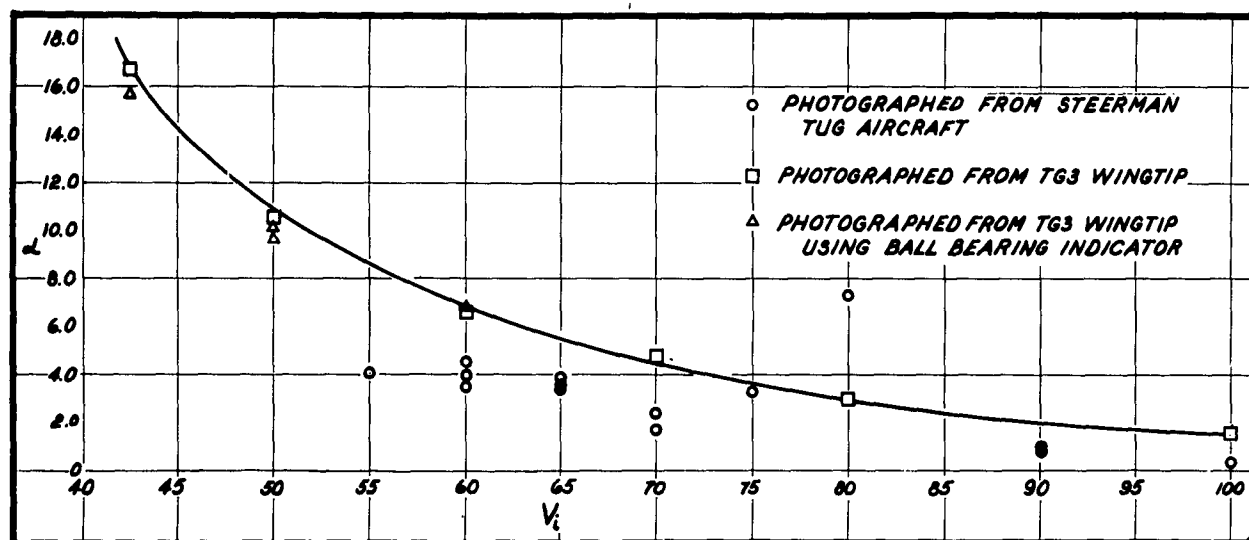


FIGURE 15 THE ANGLE OF ATTACK INDICATOR CALIBRATION CURVE.

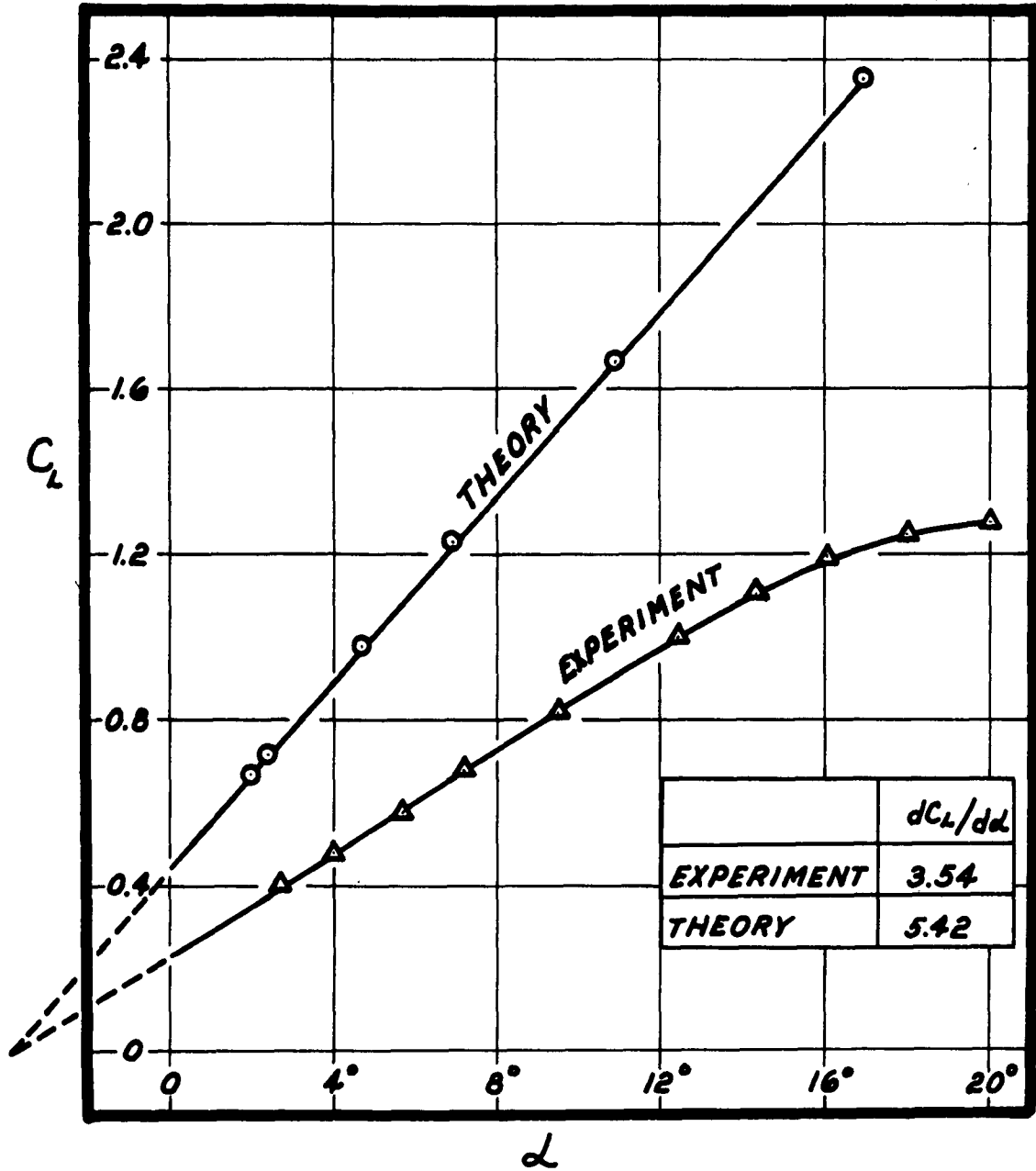


FIGURE 16 AIRFOIL SECTION LIFT COEFFICIENT AGAINST ANGLE OF ATTACK (EXPERIMENTAL AND THEORETICAL CURVES).

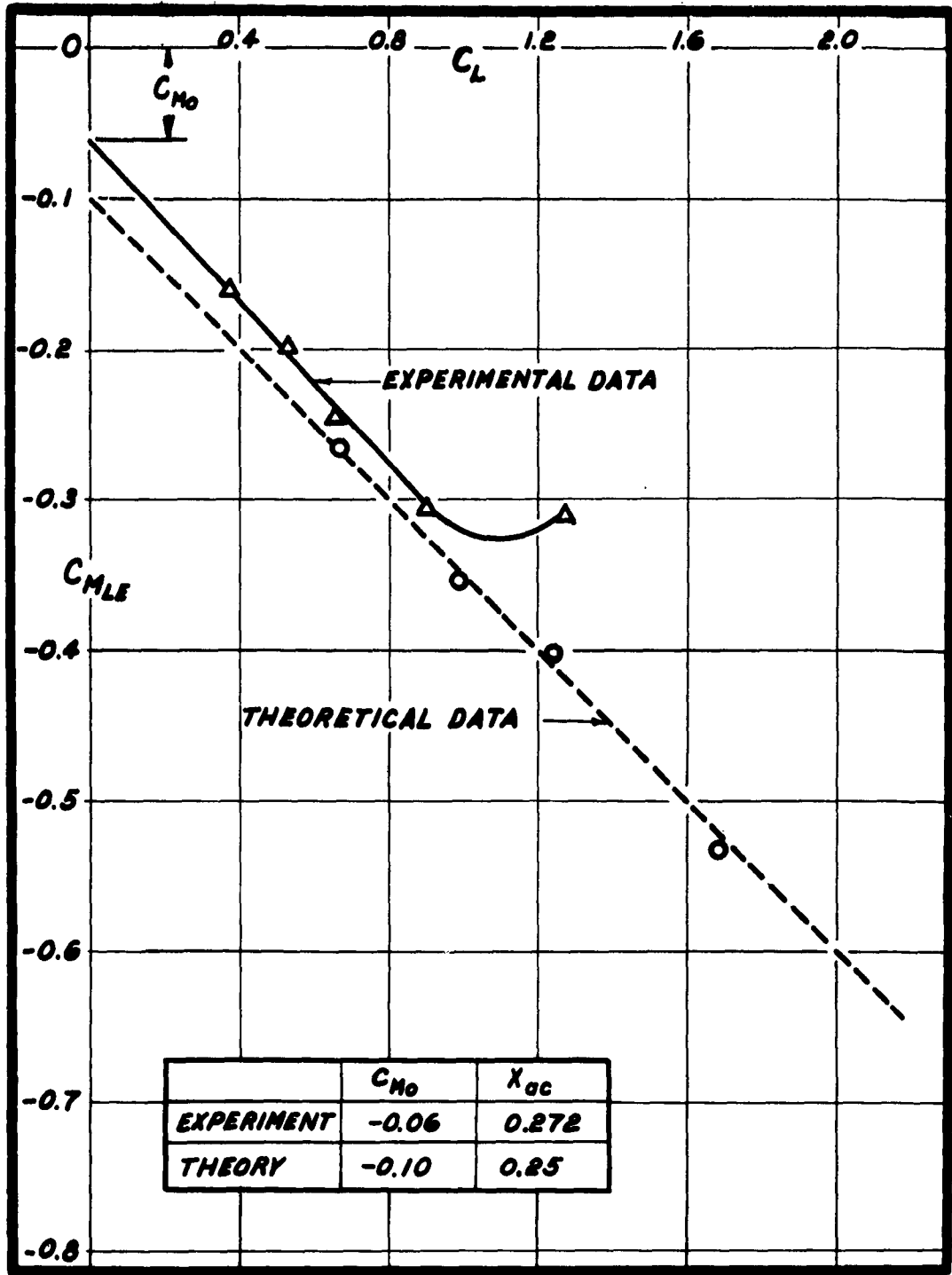


FIGURE 17 PITCHING MOMENT COEFFICIENT CURVES.

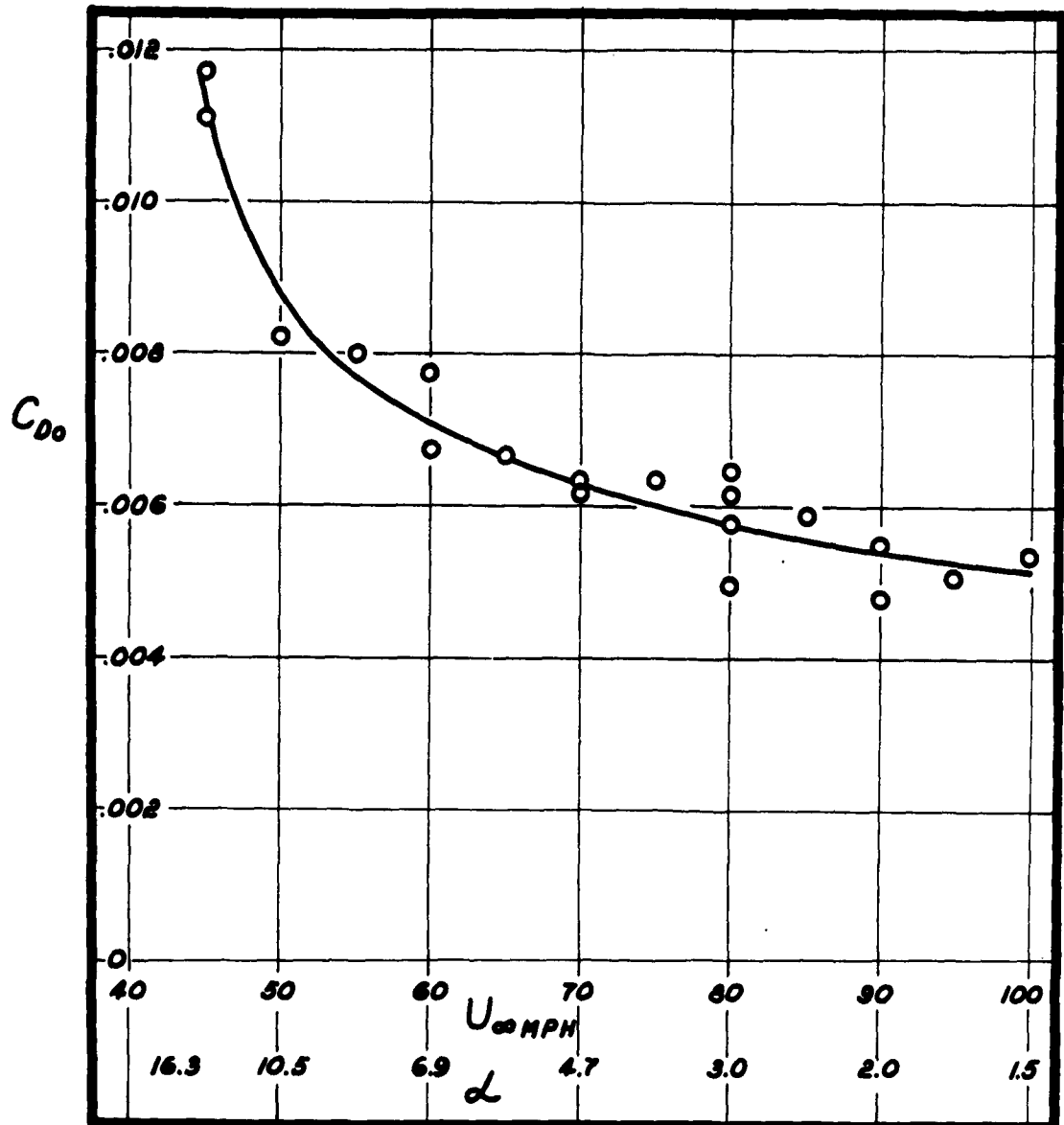


FIGURE 18 PROFILE DRAG CURVE, MARVEL AIRFOIL SECTION.

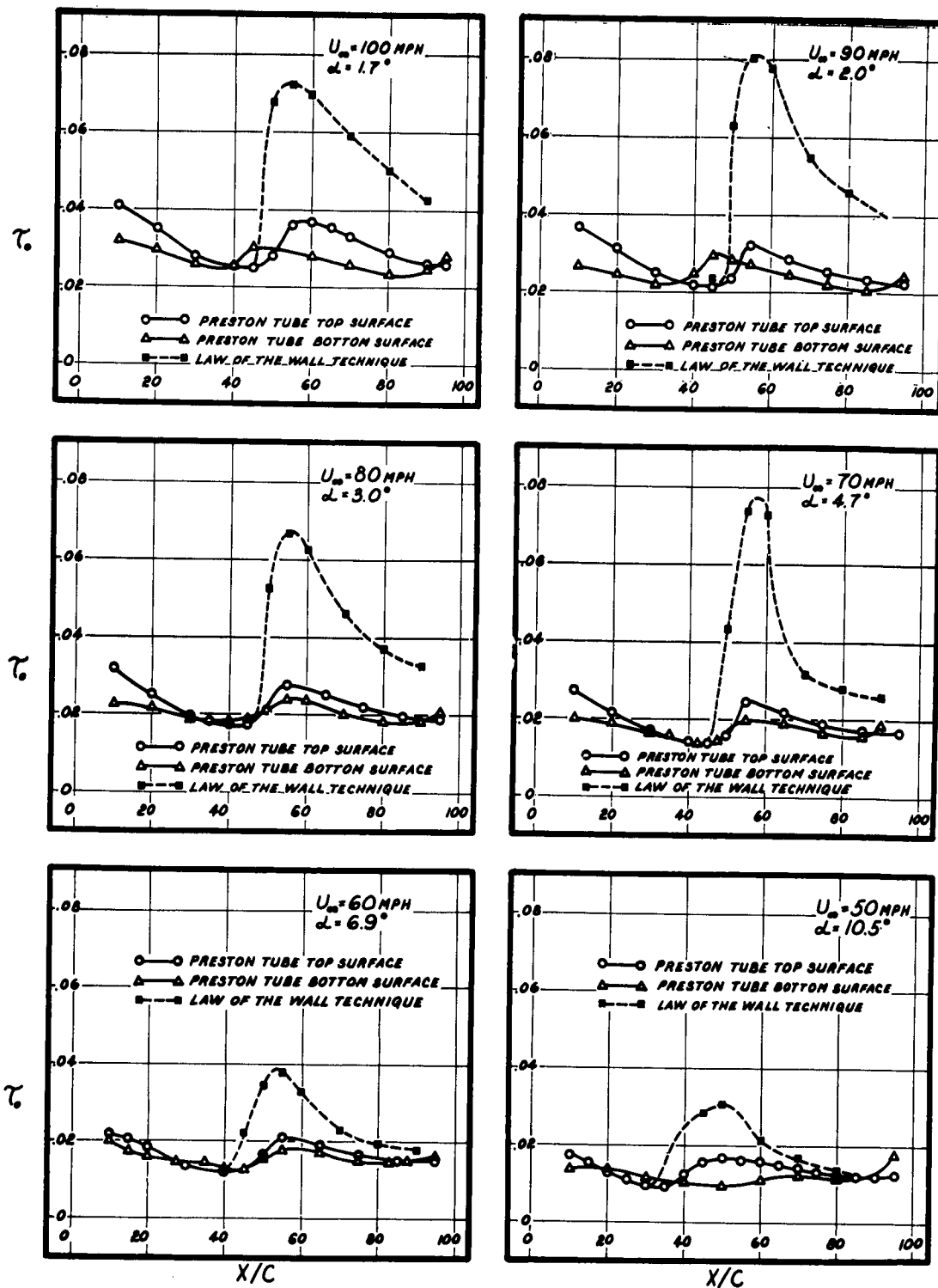


FIGURE 19 SURFACE SHEAR CURVES AT VARIOUS ANGLES OF ATTACK.

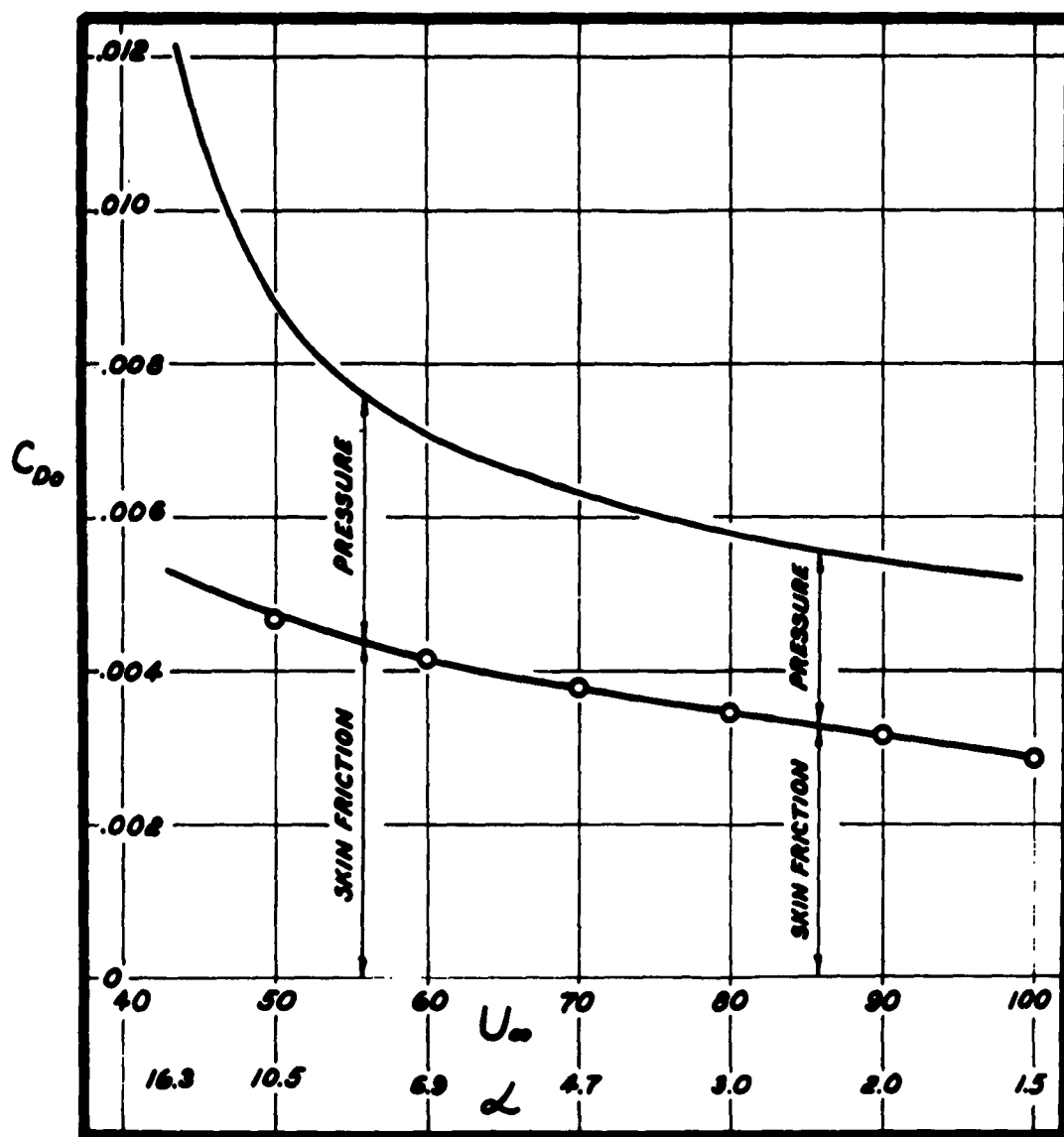


FIGURE 20 PROFILE DRAG BREAKDOWN INTO SKIN FRICTION AND PRESSURE DRAG COMPONENTS.

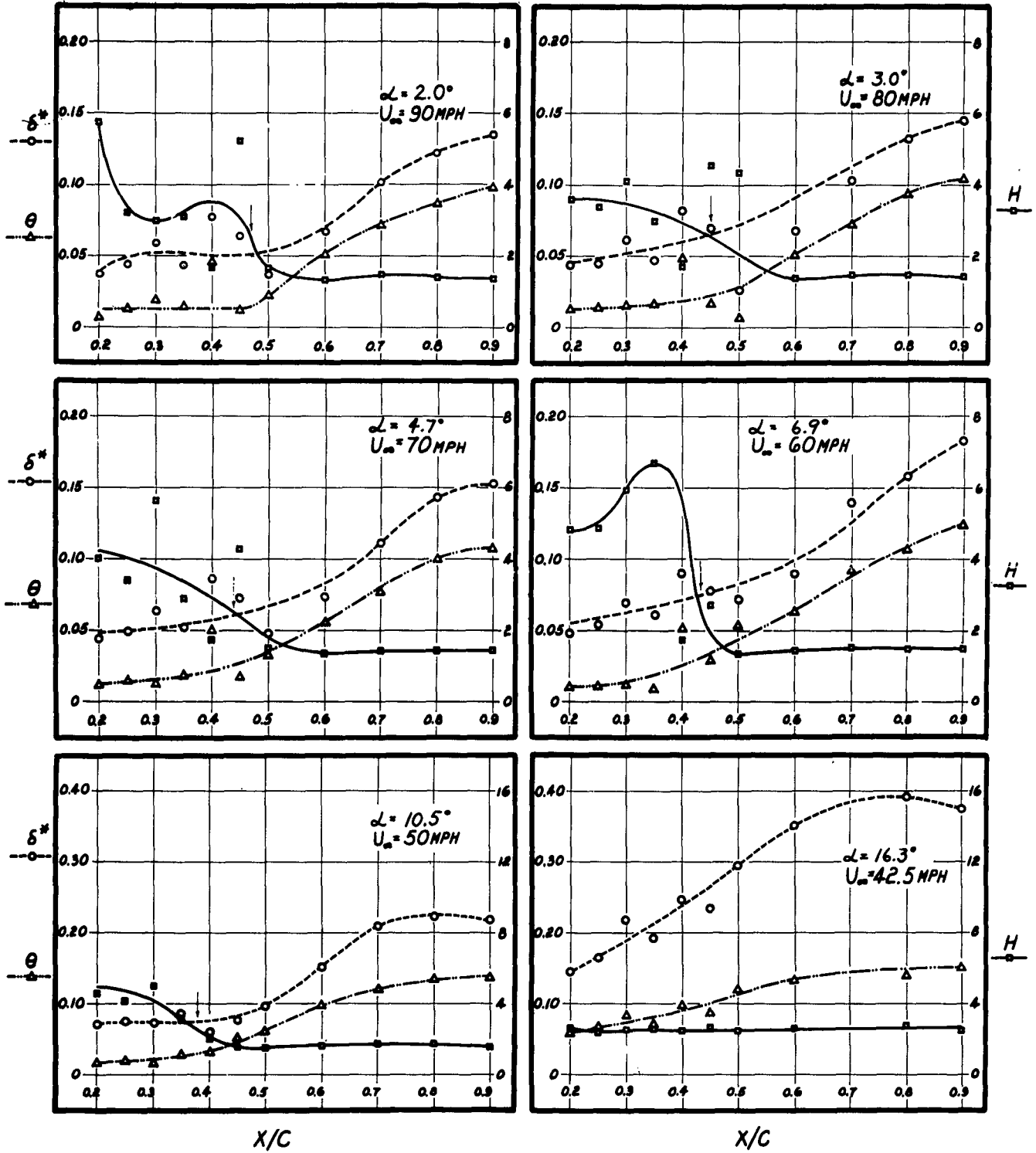


FIGURE 21 CHORDWISE DEVELOPMENT OF δ^* , θ AND H ON THE UPPER SURFACE OF THE GLOVE SECTION.

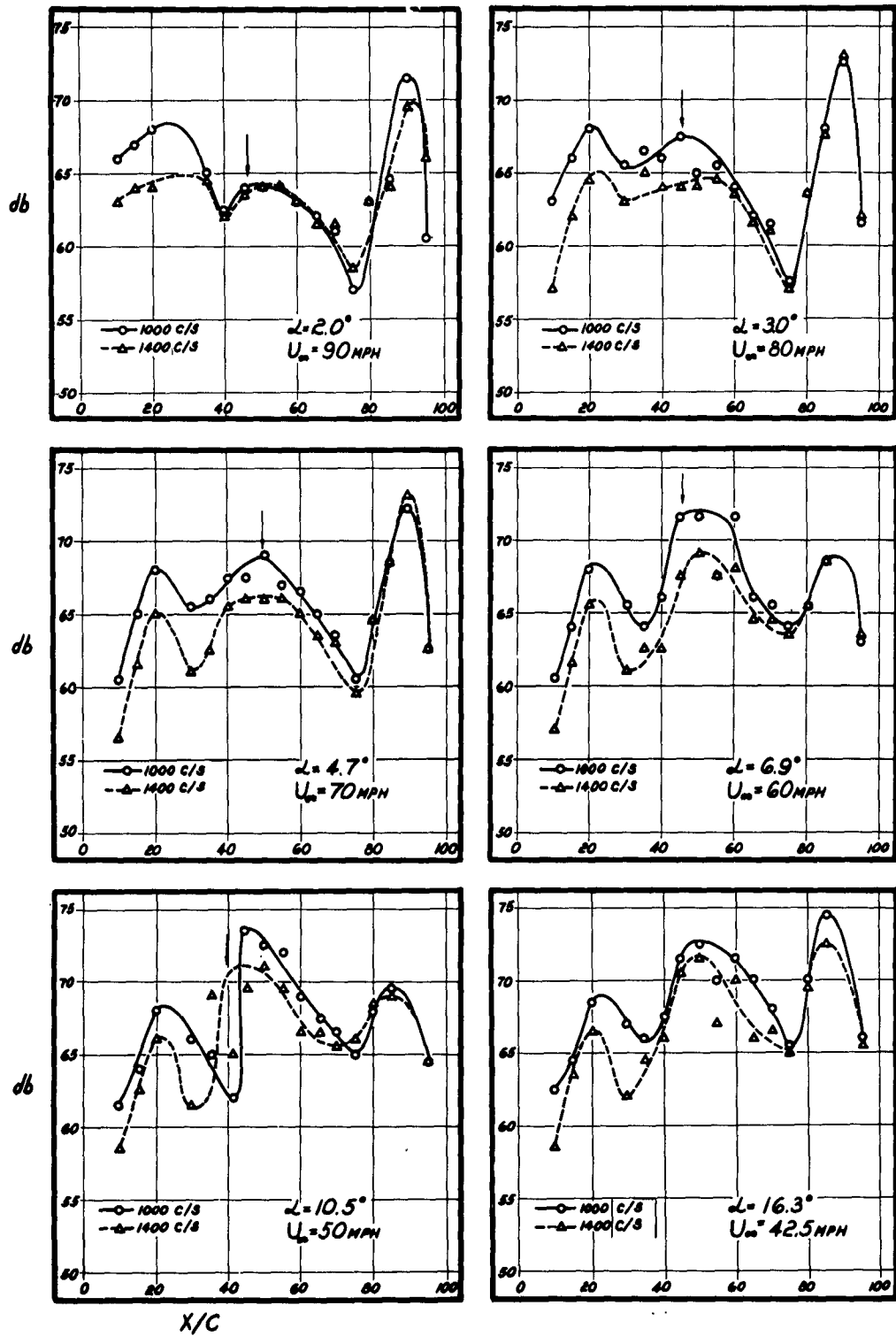


FIGURE 22 CHORDWISE DISTRIBUTION OF SOUND LEVEL INTENSITY.

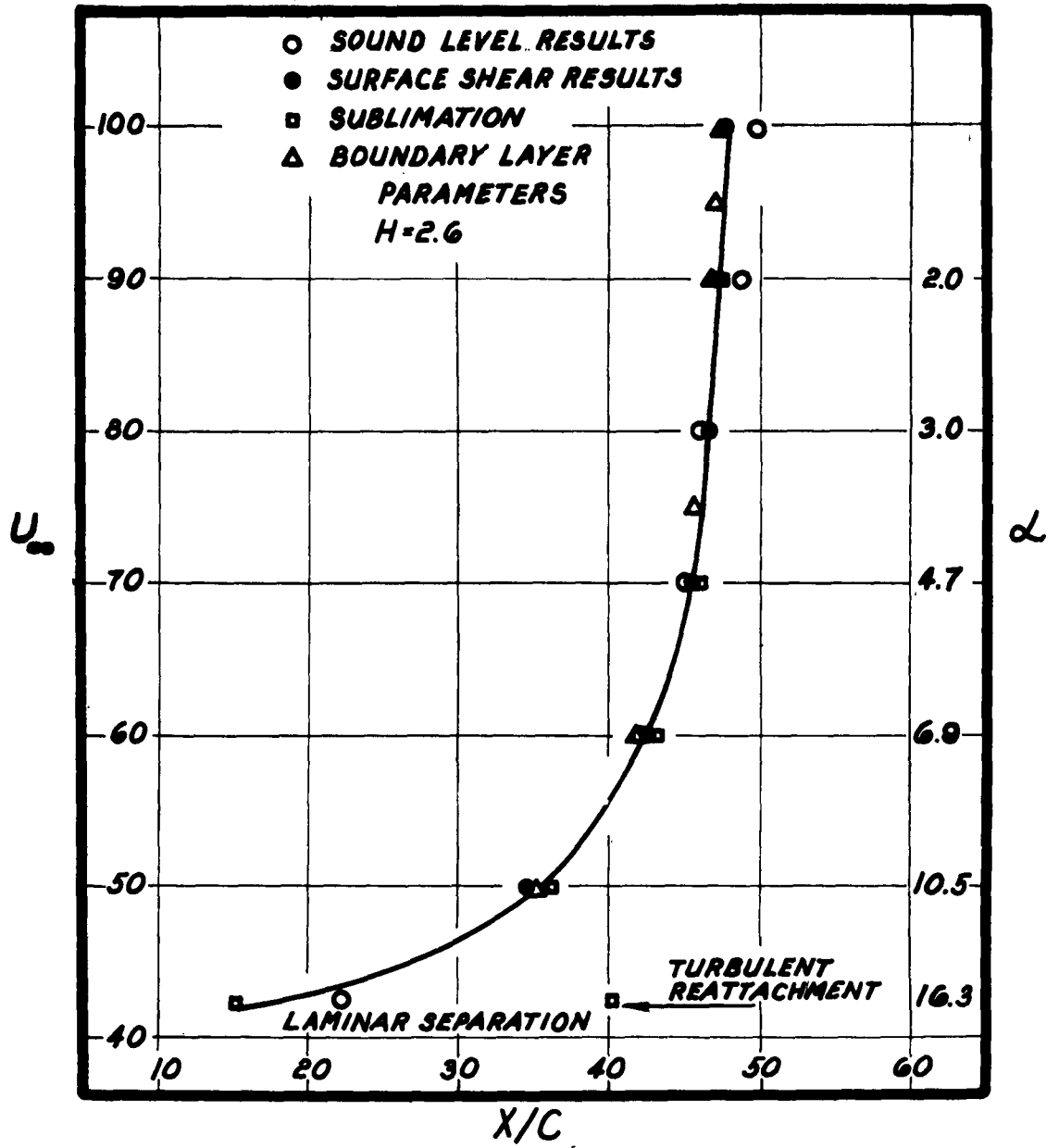


FIGURE 23 TRANSITION CURVES, UPPER SURFACE OF GLOVE SECTION.

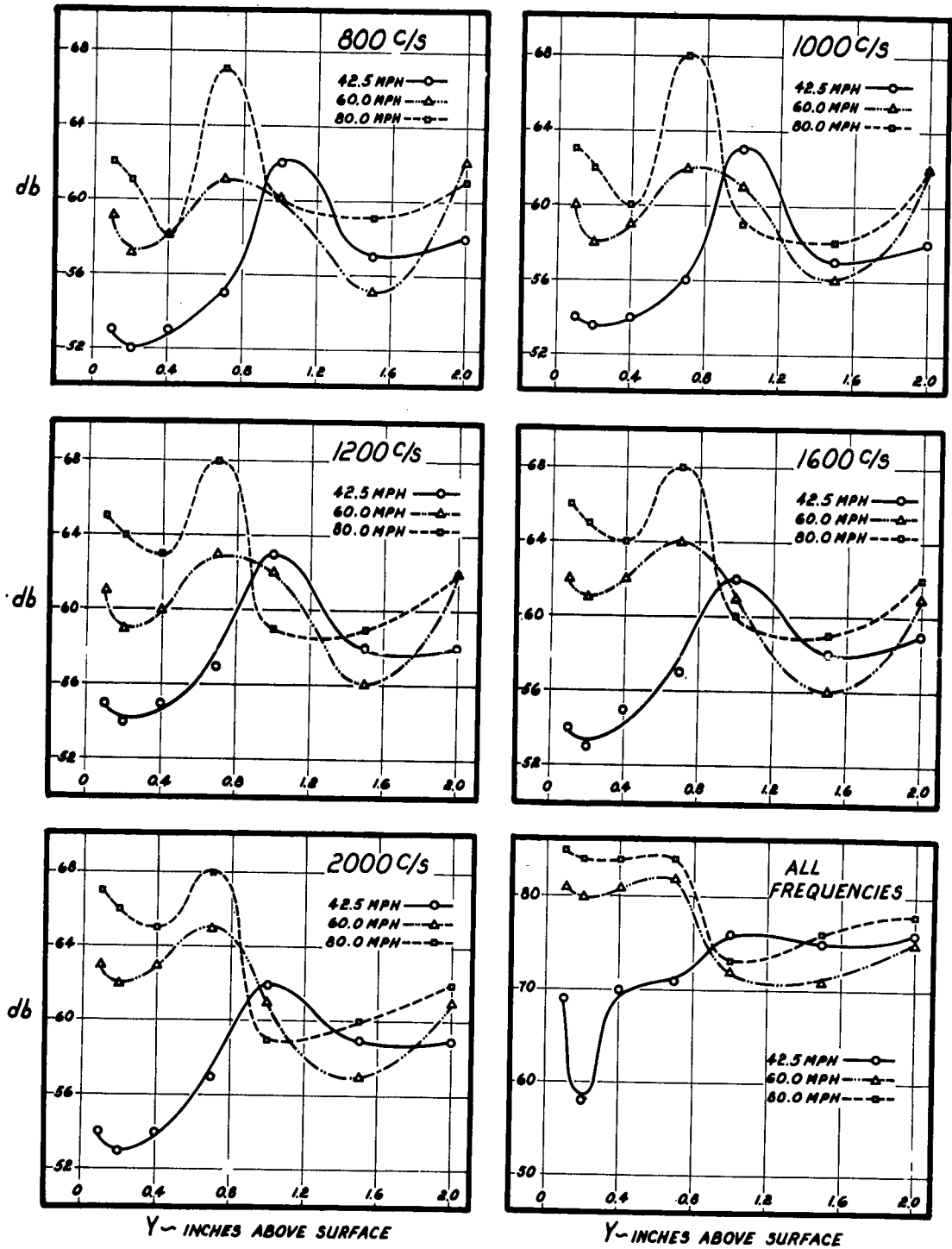


FIGURE 24 SOUND LEVEL INTENSITY BOUNDARY LAYER PROFILES AT VARIOUS AIRSPEEDS AND FREQUENCIES RECORDED AT THE 90% CHORD POSITION ON THE UPPER SURFACE.

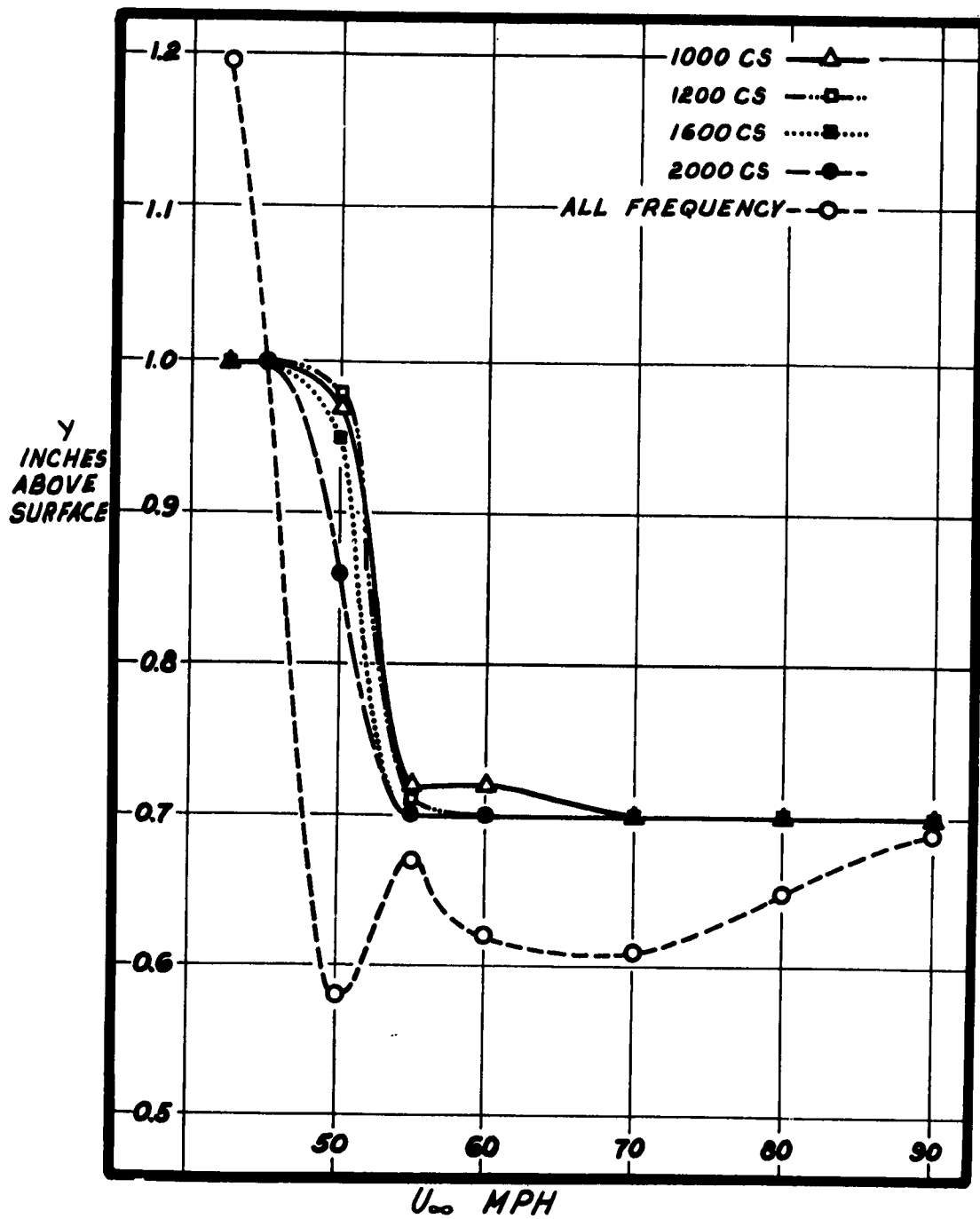


FIGURE 25 HEIGHT OF THE BOUNDARY LAYER ABOVE THE SURFACE AT VARIOUS AIRSPEEDS AT THE 90% CHORD POSITION.



FIGURE 26 POSSIBLE SOLUTION TO THE LEADING EDGE SEPARATION PROBLEM; DROOPED LEADING EDGE.